Osteogenic-differentiated Mesenchymal Stem Cell-secreted Extracellular Matrix as a Bone Morphogenetic Protein-2 delivery system for ectopic bone formation

Nathanael Larochette, Hanane El-Hafci, Esther Potier, Niclas Setterblad, Morad Bensidhoum, Hervé Petite, Delphine Logeart-Avramoglou

Osteogenic-differentiated mesenchymal stem cell-secreted extracellular matrix as a bone morphogenetic protein-2 delivery system for ectopic bone formation

Authors : Nathanael LAROCHETTE[a,b], Hanane EL-HAFCI [a,b], Esther POTIER[a,b], Niclas SETTERBLAD[c], Morad BENSIDHOUM [a,b], Hervé PETITE [a,b], Delphine LOGEART-AVRAMOGLOU [a,b]*

Affiliations:
a Université de Paris, CNRS, INSERM, B3OA, Paris, France
b Ecole Nationale Vétérinaire d'Alfort, B3OA, Maisons-Alfort, France
c Plateforme Technologique Saint-Louis, Université de PARIS, IRSL, INSERM, Paris, France

Key words: BMP-2 delivery system; Bone regeneration; Extracellular matrix; Mesenchymal stem cells; in vivo

To cite this article: Nathanael Larochette, Hanane El-Hafci, Esther Potier, Niclas Setterblad, Morad Bensidhoum, Hervé Petite, Delphine Logeart-Avramoglou. *Osteogenic-differentiated mesenchymal stem cell-secreted extracellular matrix as a bone morphogenetic protein-2 delivery system for ectopic bone formation*. Acta Biomaterialia, Volume 116, 2020, Pages 186-200, https://doi.org/10.1016/j.actbio.2020.09.003.
Document Version: Accepted manuscript including changes made at the peer-review stage.

Abstract: While human bone morphogenetic protein-2 (BMP-2) is a promising growth factor for bone regeneration, a major challenge in biomedical applications is finding an optimal carrier for its delivery at the site of injury. Because of their natural affinities for growth factors (including BMP-2) as well as their role in instructing cell function, cultured cell-derived extracellular matrices (ECM) are of special interest. We hereby hypothesized that a "bony matrix" containing mineralized, osteogenic ECM is a potential efficacious carrier of BMP-2 for promoting bone formation and, therefore, compared the efficacy of the decellularized ECM derived from osteogenic-differentiated human mesenchymal stem cells (hMSCs) to the one obtained from ECM from undifferentiated hMSCs. Our results provided evidence that both ECMs can bind BMP-2 and promote bone formation when implanted ectopically in mice. The osteoinductive potential of BMP-2, however, was greater when loaded within an osteogenic MSC-derived ECM; this outcome was correlated with higher sequestration capacity of BMP-2 over time in vivo. Interestingly, although the BMP-2 mainly bound onto the mineral crystals contained within the osteogenic MSC derived-ECM, these mineral components were not involved in the observed higher osteoinductivity, suggesting that the organic components were the critical components for the matrix efficacy as BMP-2 carrier.

Graphical abstract

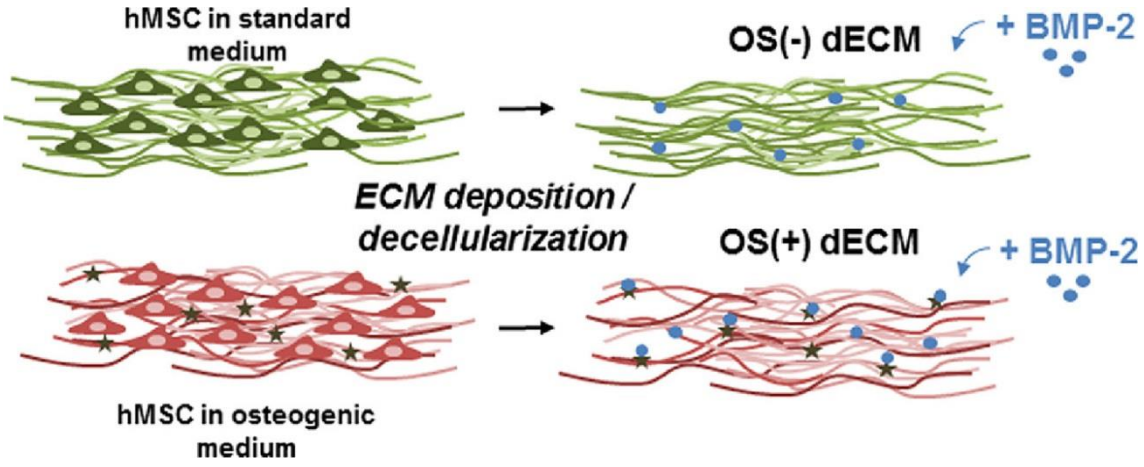

Introduction

Orthopedic tissue engineering applications and regenerative strategies aim at improving current clinical practices for repairing large bone defects resulting from trauma, congenital malformations, and surgical resections. The combination of osteoinductive growth factors and/or stem/progenitor cells (such as mesenchymal stem cells; MSC) with osteoconductive biomaterials remains a promising approach to promote bone regeneration [1].

Osteoinductive growth factors stimulate new bone tissue formation and, when loaded within appropriate delivery systems, represent attractive treatment options for promoting bone regeneration and repair. Among such systems, bone morphogenetic protein-2 (BMP-2) is the most potent osteoinductive growth factor involved in the early stage of bone formation and repair [2]. Endogenous BMP-2 is important for normal bone homeostasis, is upregulated immediately following bone trauma, and actively contributes to the recruitment, proliferation, and differentiation of osteoprogenitor cells during the bone healing process [3,4]. For these reasons, products containing recombinant BMP-2 loaded in bovine, collagen-type-I matrix (as a carrier) have been used in orthopedic applications (such as spinal fusions, and non-unions) [5,6] and in oral surgery. BMP-2-based products, however, have had complications that limited the extent of their clinical use; in fact, BMP-2 promoted bone formation in a dose-dependent manner, but delivery of supraphysiological doses (i.e. several milligrams in humans) induced pathological events (such as significant osteolysis, heterotopic ossifications, immunological reaction and tumorigenesis) [7], that have been reported primarily in spinal application in humans [8,9]. Some reviews on the safety of BMP-2 in spinal surgery concluded an incidence of 10–50% adverse events depending on the type of clinical application [10,11]. Additionally, recent studies provided evidence that the degree of the early inflammatory response of collagen sponge combined with BMP-2 may be associated with the physical and chemical properties of the carrier material itself [12]. As a result, intensive research studies are still ongoing in order to determine the "ideal" material carrier of BMP-2, which can deliver the minimum required dose for improving bone repair with fewer, and lesser, side effects. To this aim, a large number of material carriers and delivery systems have been investigated for controlled, localized, and sustained release of BMP-2. The materials tested for such applications include mostly calcium phosphate (CaP)-based ceramics, biodegradable synthetic and natural polymers, and composites thereof (see [13] for review).

Because of their natural affinities for BMPs, extracellular matrix (ECM)-derived components such as heparin/heparin sulfate [14], fibronectin [15], fibrillin [16] and collagen [17] are of special interest. Indeed, physiologically, BMP-2 bioavailability and signaling are tighly regulated by either low or high binding affinity to ECM components [18]. Such BMP–ECM interactions direct and control BMP gradients during organism development and also define extracellular BMP concentrations within the bone micro-environment. These aspects of the physiological milieu have been the motivation of some tissue-engineering strategies, which combine recombinant BMPs with naturally-occurring ECM components within either hydrogels or as material surface coatings, in order to modulate the growth factor release kinetics, and to enhance the bone forming capacity of BMP-containing delivery systems [15,17,19,20].

Incorporating either single or more naturally-occurring ECM components or peptides in tissue engineered scaffolds has, however, limitations and fails to mimic the molecular complexity and organization of native tissue matrices. In fact, the ECMs derived from either tissues or cultured mammalian cells, are complex and highly-organized assemblies of macromolecules including collagens, fibronectin, laminin, and various types of glycosaminoglycans (GAGs) and proteoglycans. Thus, in addition to being involved in the binding, sequestration and stabilization of signaling molecules, the ECMs also provide the required substrates for anchorage-dependent cell adhesion, and cues for cell survival, migration, proliferation, and differentiation, i.e., the essential processes for new tissue formation, homeostasis and repair [21].

Recently, use of ECMs derived from osteogenic progenitor cells (such as MSCs) has gained increasing interest in the field of bone tissue engineering, especially for the purpose of expanding the cells and maintaining their phenotype (see [22] for review). Cultured cell-derived ECM, therefore, may not only serve as therapeutic platforms for controlling delivery of exogenous-binding growth factors, but can also instruct the phenotype of host progenitor cells through numerous scaffold-contained biological cues. Very few studies, however, have examined the potential role of cell-derived matrices as BMP-2 delivery systems, and most importantly, none of them assessed the performance of such systems in vivo [23], [24], [25].

For this reason, in the present study, we assessed the efficacy of ECMs secreted by human bone marrow-derived MSCs as BMP-2-delivery systems both in vitro and in vivo. Because BMP-2 has affinity for CaP minerals [26], [27], [28] and the composition and distribution of specific ECM components, which vary with the stage of cell differentiation, may also affect cell fate and function, we hypothesized that a "bony matrix" containing mineralized, osteogenic ECM is a potential efficacious carrier of BMP-2 for promoting bone formation in vivo. For this purpose, we compared the efficacy of decellularized ECM, derived from osteogenic-differentiated human MSCs (hMSCs), to that of decellularized ECM, derived from undifferentiated hMSCs, regarding BMP-2 retention and resultant outcomes on bone formation in vivo in mice.

Materials and Methods

Human Mesenchymal Stem Cell (hMSC) isolation and culture

hMSCs were harvested from bone marrow obtained as discarded tissue during routine bone surgery from 3 donors (1 woman and 2 men; 15, 22 and 31 years-old, respectively) at the Lariboisiere Hospital, Paris, France. The tissues were collected with the respective donor's consent in agreement with Lariboisiere Hospital regulations. hMSCs were isolated from each donor's bone marrow, cultured under "standard" cell culture medium (specifically, alpha-Minimum Essential Medium (α-MEM, Sigma) containing 10% fetal bovine serum (FBS; PAA Laboratories) and 1% antibiotics (PAA Laboratories)) and characterized by expression of select CD markers (specifically, positive for CD90, CD73, CD105 and negative for CD45; data not shown) as previously described [29]. At passage 1, the hMSCs from each donor were pooled at an equal ratio, and used for experiments up to passage 6.

Preparation of decellularized, cell-secreted, extracellular matrices (ECMs)

For in vitro experiments, cell-secreted ECMs were prepared in individual wells of 48-well plates. HMSCs were seeded at 25,000 cells/cm² and cultured either in standard cell culture medium supplemented with 1 mM ascorbic acid 2 phosphate (Sigma Aldrich) or in osteogenic cell culture medium (Osteogenic bullet kit; Lonza) for 21 days; in the rest of the present manuscript, these preparations are referred to as OS(-) ECM and OS(+) ECM, respectively. The cell layers were then rinsed twice with phosphate-buffered saline (PBS) and decellularized by treatment with 20 mM NH4OH / 0.25% Triton X-100 at room temperature for 10 min. The resulting decellularized ECMs (dECM) were rinsed twice with PBS and air-dried in a sterile hood overnight. The DNA contents within each ECM were quantified before and after decellularization and results indicated that 17% and 26% of DNA remained in the OS(-) and OS(+) matrices after the decellularization treatment, respectively. dECM-containing plates were stored in sealed bags at −20 °C until further use in experiments.

For in vivo experiments, hMSCs were cultured onto 3D polycaprolactone (PCL) scaffolds (3D Biotek PCL 24 well-plate insert with open and interconnected pore size of 300 µm; Sigma); The adhesion of hMSCs (previously infected with a Luc-ZsGreen lentivirus ([30]; pRRLsin-MND-Luc-IRES2-ZsGreen-WPRE; TBMCore; Bordeaux, France) onto 3D PCL scaffolds was monitored using fluorescent microscopy (NIKON TE2000, λ ex = 472/30 nm -DM 495 nm, λ em = 520/35 nm), while their proliferation under standard cell culture medium was monitored non-destructively by bioluminescence imaging (IVIS Lumina II, Perkin Elmer) for 3 weeks. The 3D-PCL-dECMs were prepared using the same procedures as those described in preparing dECMs in 48-well plates (referred to as 2D-dECMs).

A set of experiments was performed using decalcified 2D- and 3D-PCL-OS(+) dECMs. To this aim, OS(+) dECMs were treated with 0.6 M ethylene diamine tetra acetic acid (EDTA) for 24 h, then rinsed in PBS before use.

Characterization of cell-secreted, extracellular matrices (ECMs) and decellularized extracellular matrices (dECMs)

The fibrillar collagen and glycosaminoglycans (GAG) contents in the ECMs of interest to the present study were both assessed by staining with Sirius Red/Fast Green FCF [31] and safranin O, respectively. Briefly, either 2D- ECMs (both decellularized and not) or 3D-PCL-dECMs were fixed using 4% paraformaldehyde and stained using either a saturated picric acid solution containing 0.1% w/v picrosirius red (Direct red 80, Sigma Aldrich) and 0.1% Fast Green FCF (Sigma Aldrich) or using 0.5% Safranin O in Sodium Acetate (pH 5.2) for 1 h. After extensive rinsing with tap water, the Sirius Red/Fast Green stains were extracted using 0.1 M NaOH / Methanol (50/50; v/v) and the absorbances for the extracted Sirius Red and Fast Green FCF were measured at 605 nm and 540 nm, respectively. The Safranin O stain was extracted using 72 mM HCl/Ethanol (50% v/v) and its absorbance was measured at 530 nm. The fibrillar collagen content was calculated using the formula: DO540 - (DO605 x 0.291). All absorbance values were reported in arbitrary units. The level of ECM mineralization within 2D-ECMs was assessed by measuring the respective calcium content. Each matrix was decalcified using 0.1 M HCl for 2 h; the calcium content in the resulting supernatants was assessed using a Ca-Kit (Biomérieux). The presence of calcium containing deposits in the 3D-PCL OS(+) dECM was detected by staining the scaffold using the Alizarin red (AR) method. The surfaces of the 2D-dECMs (prepared onto coverslips (Thermanox, Thermofisher)) and of the 3D-PCL dECMs were examined using scanning electronic microscopy (Zeiss ULTRA 55 FEG-SEM) [32]. The ratio of calcium-to-phosphorous content of the mineral crystals present on OS(+) dECM was determined using Backscattered-electron (BSE) imaging and Energy-dispersive X-ray spectroscopy (EDX) analysis.

Select functions of cultured hMSCs seeded onto dECMs

The adhesion, proliferation, and osteogenic differentiation of hMSCs cultured onto either 2D-dECMs or tissue-culture-plastic (TCP) were assessed. To visualize adherent cells, the hMSCs were stained using 1 µM Cell tracker Orange (Life Technologies) in standard cell culture medium 4 h after cell seeding (15,000 cells/cm²), visualized using a fluorescence NIKON TE-2000 microscope (λ ex= 543/22 nm; λ em= 593/40 nm) and photographed. To assess the cell proliferative rates, hMSCs were cultured in standard cell culture medium for 1, 5, 9 and 16 days, then rinsed with PBS, trypsinized, and analyzed using an Attune Flow Cytometer (Applied Biosystems) using a forward vs. side scatter gating. To assess the osteogenic differentiation, the seeded hMSCs were cultured either in osteogenic (Lonza) or in standard cell culture media with a medium change every 3 days. The alkaline phosphatase (ALP) activity in hMSC lysates was determined after 7 days of culture as previously described [32]. After 14 days of hMSC culture, gene expression was determined using Taqman probes for hALP (Hs01029144_m1), hRUNX2 (Hs00231692_m1) and hIBSP (Hs00173720_m1) as previously described [29] and using the MyiQ™ Single-Colour Real-Time PCR Detection System (Biorad).

Fluorescence labeling of BMP-2

Recombinant human BMP-2 powder (InductOs® 12 mg; Medtronic) was reconstituted by dissolution in sterile 1 mM HCl (to obtain a concentration greater than 100 µg/ml), aliquoted, and kept at −80 °C until further use in experiments. The initial BMP-2 concentration was assessed by UV detection at 280 nm using a NanoDropTM1000 UV–Vis Spectrophotometer (NanoDrop Technologies, Inc.) with the extinction coefficient fixed at 1.41 absorbance units per mg/ml. For all experiments, the BMP-2 used was further diluted in PBS containing 0.5% Bovine Serum Albumin (Sigma-Aldrich).

Two fluorescently-labelled-BMP-2 solutions were prepared by coupling BMP-2 either with Dylight 488 N-hydroxysuccinimide - ester (BMP-2^{DL488}) or with Dylight 800 N-hydroxysuccinimide-ester (BMP-2^{DL800}) (both from Thermofischer Scientific) for in vitro and in vivo studies, respectively. Briefly, 1 mg BMP-2 was dialysed against 1 mM HCl for 24 h and its pH adjusted to 8.5 using 1 M sodium borate. Either Dylight 488 NHS ester or Dylight 800 NHS ester was added to the respective BMP-2 solution in a 2- and 6-fold molar excess, respectively; the resultant mixtures were maintained at room temperature for 2 h. After adjusting the pH at 3 (using HCl), the labelled protein was dialysed against 1 mM HCl. The concentrations of both BMP-2^{DL488} and BMP-2^{DL800} were determined using the Pierce BCA protein assay (Thermofischer Scientific).

Visualization of BMP-2 bound within dECMs

The 2D-dECMs (prepared onto coverslips) tested were incubated with 145 ng of BMP-2^{DL488} in PBS containing 0.5% BSA, for 30 min at room temperature and then washed 3 times in

PBS. The OS(-) 2D-dECMs structure containing high level of collagen was visualized using Second-harmonic generation (SHG) imaging. Images were acquired using AxioExaminer Z1 ZEISS LSM780 confocal microscope (Zeiss, Oberkochen, Germany). The IR laser was tuned at 860 nm and 20.9% output power.

The OS(+) 2D-dECMs were sequentially observed using a NIKON TE2000 microscope in standard brightfield mode with a green fluorescent protein filter cube (λ ex = 472/30 nm –DM 495 nm, λ em = 520/35 nm). The BMP-2^{DL488}-containing OS(+) 2D-dECMs were then treated with 34 mM EDTA (prepared in 0.1 M phosphate buffer; pH 7.4) to dissolve the CaP crystals. Micrographs were taken at 30, 180 and 300 s after addition of the EDTA solution. The background fluorescence of OS(+) 2D-dECMs was checked in the absence BMP-2^{DL488}. Binding and localization of BMP-2 onto OS(+) 2D-dECMs previously decalcified by treatment in EDTA for 30 min was also observed.

Retention of BMP-2 into dECM and evaluation of its biological activity

The 2D-dECMs tested were immersed in 4 µg/ml BMP-2 at room temperature for 30 min; at that time, the amount of non-retained BMP-2 in the collected supernatant was quantified using a commercial ELISA kit (Human BMP-2 DuoSet; R&D system). The bioactivity of the BMP-2 retained into 2D-dECM was determined by assaying the BMP-2-induced ALP activity (a marker of osteogenic differentiation) in murine C2C12 skeletal myoblasts (American Type Culture Collection) [33]. C2C12 cells (25,000 cells/cm² in Dulbecco's modified Eagle's medium supplemented with 2% FBS) were seeded on each 2D-dECMs previously loaded with 4 µg/ml BMP-2 (and quickly rinsed with PBS-0.5% BSA), and cultured under standard cell culture conditions for 6 days. At this time, cells were rinsed using PBS and the ALP activity in each cell lysate was determined. In another set of experiments, before C2C12 cell seeding, the BMP-2-loaded 2D-dECMs were freeze-dried, and stored at 4 °C in sealed bags for either 48 h or 11 months.

In vivo studies

The osteoinductive potential of BMP-2 containing PCL scaffolds was assessed in vivo in a mouse ectopic model. Five experimental groups were designed, including 3 groups prepared with BMP-2: OS(-) and OS(+) dECM 3D-PCL scaffolds and "bare" 3D-PCL used as uncoated scaffold controls; and 2 groups (OS(-) and OS(+) dECMs) prepared without BMP-2 and used as unloaded scaffold controls (see Table 1). PCL scaffolds were immersed in 100 µl of PBS-0.5% BSA without (for scaffolds without BMP-2) or with 50 µg/ml BMP-2 at room temperature; some scaffolds were loaded with 50 µg/ml BMP-2 including 10% (w/w) of BMP-2^{DL800} (see Table 1). After 1 hour, the supernatants were discarded and the fluorescence emitted from the scaffolds loaded with the labelled BMP-2 was quantified using an IVIS Lumina II fluorescent imaging system (Perkin Elmer; λ ex = 745/10 nm / λ em = 810–875 nm). The PCL scaffolds were then implanted in eight-week-old, female, nude mice (NMRI-nu (nu/nu) obtained from JanvierLabs) as previously described [30]. The animal handling and experiments were performed in accordance with the European Directive 2010/63/EU and following protocol approval by the Ethics Committee on Animal Research (APAFIS#6607–2016070410411411).

The release kinetics of BMP-2 labelled with a near-infrared (NIR) fluorophore (BMP-2^{DL800}) from the PCL scaffolds were monitored non-invasively in vivo using the IVIS Lumina imaging system. The mice were anesthetized by inhaling isoflurane, placed in the prone position inside the detection chamber of the imaging system, and were imaged each day during the first week post-implantation and then twice-a-week for 3 weeks. Standard regions of interest surrounding each implant were delineated on the obtained fluorescent images and the total fluorescence emitted by each BMP-2^{DL800}-containing scaffold was quantified using the Living Image 3.1 software (Caliper Life Sciences). These data were normalized to those measured the day of implantation (day 0).

New bone formation induced by the BMP-2-containing PCL scaffolds was monitored in vivo using µ-CT at 2, 4 and 8 weeks post-implantation. Under anesthesia using isofluorane, the mice were scanned using a Skyscan 1176 high resolution µ-CT scanner (Bruker). Images were acquired using the following settings: voltage 50 kV, current 350 µA, exposure for 350 ms, and 0.7° rotation-step settings, through a 0.5 mm-thick aluminum filter. The initial pixel size at these settings was 35.4 µm. The scanned images of each implant were reconstructed as a stack of slices using Nrecon software (Bruker). The new bone volume per each PCL scaffold was determined using the CTAn software (v1.15.4.0; Bruker; grayscale threshold values within 51–255). The binarization threshold was determined by Otsu's method [34], based on histograms of 3D µCT scans of BMP-2 containing-PCL scaffolds.

Eight weeks post-implantation, the mice were sacrificed through injection of lethal doses of pentobarbital (Dolethal®; Vetoquinol). The PCL scaffolds were excised and processed for undecalcified histology [32]. Each sample was then cut into 500 µm-thick sections and stained using Stevenel's blue and Van Gieson Picrofuchsin red for subsequent histological analyses.

Statistical analyses

Numerical results were reported as average ± standard error of the mean. Statistical analyses were conducted using the Statgraphics Centurion version XV.2 (Statpoint, Inc.). One-way ANOVA followed by Tukey's posthoc test was used to compare means of more than two groups. The quantitative kinetics data were analyzed using two-ways ANOVA followed by Tukey's posthoc test. For all analyses, differences at $p<0.05$ were considered as statistically significant. For the analysis of the BMP-2^{DL800} release kinetics in vivo, a non-compartmental analysis was used to calculate areas under the curve (AUC) and areas under the moment curve (AUMC). The mean residence time (MRT) for the implanted BMP-2^{DL800} was calculated by the ratio AUMC/AUC. An exponential model was used to obtain half-lives ($t_{1/2}$); $C(t) = C_0 e^{-Kt}$ where C(t) = fluorescence at time t; K = rate constant, and $t_{1/2} = 0.693/K$.

Results

Biochemical characterization of both ECMs and dECMs

The contents of the major ECM components (i.e., total protein, fibrillar collagen, and GAGs) secreted by the hMSCs cultured either in a standard cell culture medium (OS(-)) or in an osteogenic cell culture medium (OS(+)) for 21 days were quantified before, and after, ECM decellularization (Fig. 1A). The results provided evidence that, compared to results obtained when the ECM was formed under OS(-) conditions, production of ECM under osteogenic conditions (OS(+)) led to a significant reduction in total protein (−2.3 fold), fibrillar collagen (−3.9 fold), and GAG (−1.6 fold) contents. In both OS(-) and OS(+) cases, the decellularization

process removed a large amount of both total protein (−2.8 to −3.0 fold) and GAG (−2.6 to −3.1 fold) contents, but did not affect the collagen content of the ECMs. After decellularization, the OS(+) dECMs contained 2.1-fold less total proteins, and 6.8-fold less fibrillar collagens but the same amount of GAGs compared to OS(-) dECMs. SEM examination of the dECMs revealed differences in the matrix structure (Fig. 1B). While the OS(-) dECMs contained a highly dense network of entangled thin fibers (size in the order of nanometers), the OS(+) dECMs contained more widely spaced, but thicker, fibers with numerous anchored crystals; atomic chemical analysis of these crystals confirmed their calcium phosphate form with a Ca/P ratio of 1.5. Measurement of the calcium contents in each ECM and dECM tested further confirmed the calcified nature of the OS(+) matrices; there was no difference, however, in the calcium contents of the OS(+) ECMs and OS(+) dECMs providing evidence that the decellularization process did not extract the CaP crystals from the OS(+) matrices.

hMSC functions onto dECMs

In order to investigate the fate of osteoprogenitor cells on dECMs, adhesion, proliferation, and osteogenic differentiation of hMSCs cultured onto either OS(-) or OS(+) dECMs were determined and compared to results obtained when hMSCs were cultured on tissue culture plastic substrate (TCP). Examination of hMSCs labelled with the Cell tracker Orange dye 4 h post-seeding indicated that the hMSCs seeded onto the two dECMs tested were more spread and had numerous extensions compared to hMSCs seeded on TCP which displayed rounder shapes (Fig. 2A). The proliferation rate of hMSCs was the highest on OS(+) dECMs and lowest onto TCP; the proliferative doubling time of hMSCs cultured on the OS(+), OS(-) and TCP substrates were 5.4, 9.8 and 11.0 days, respectively (Fig. 2B). The osteogenic differentiation of hMSCs cultured onto the substrates tested for 7 days was assessed by quantifying the ALP activity (Fig. 2C). Under standard cell culture medium, the ALP activity in all cultured hMSCs was minimal, and was lower than under osteogenic cell culture medium. Such ALP activity was higher in hMSCs cultured on the OS(-) dECM compared to the other substrate groups tested. Expression levels of osteogenic genes by hMSC cultured in osteogenic medium for 14 days were also investigated (Fig. 2D). At that time, hMSCs cultured onto OS(-) dECM expressed higher levels of the early (*hRunx2* and *hALP*) and late (*hIBSP*) osteogenic markers compared to those obtained when these cells were cultured on OS(+) dECM (Fig. 2D). It is worthy to note that the gene expression profiles were similar at day 7 (with a lower level of expression) to those obtained at day 14 (data not shown). Altogether, these results indicated that both dECM substrates promoted hMSC adhesion and proliferation; the OS(+) dECM, however, better promoted hMSC proliferation, while OS(-) dECM better promoted the hMSC osteogenic differentiation.

Localization and bioactivity of BMP-2 loaded within dECMs in vitro

Localization of BMP-2 bound onto dECMs was visualized using fluorescently-labelled-BMP-2 (BMP-2^{DL488}). Taking advantage of the fibrillar collagen-rich structure of the OS(-) dECM, the matrix was visualized using SHG imaging (Fig. 3Aa). Simultaneous imaging of BMP-2^{DL488} and collagen fibrils showed that BMP-2 was homogeneously distributed within the dECM in the form of both soluble protein (appears as diffuse fluorescence) and protein aggregates (appear as bright spots) (Fig. 3Ab-c). Because the OS(+) dECM did not contain enough collagen fibrils to be visualized by SHG imaging, the mineralized matrix (containing grainy mineral deposits) was observed using brightfield microscopy (Fig. 3Ba). Imaging of the BMP-2^{DL488} revealed a green fluorescent pattern that mainly colocalized with the mineral deposits (Fig. 3Bb). To further confirm BMP-2 adsorption onto the CaP minerals, the BMP-2-containing OS(+) dECMs were treated with EDTA for decalcification. Live imaging in brightfield mode confirmed the dissolution of the mineralized crystals (Figs. 3Ba-c-e), while the fluorescence imaging showed a strong, but not total, attenuation of the signal after 300 s of EDTA treatment (Fig. 3Bb-d-f). As expected, the profiles of the intensity values indicated a higher loss (~60–80%) of fluorescence within mineral-containing areas compared to lower loss (~20–30%) in the mineral-free areas (Supplementary Figure 1). Interestingly, addition of BMP-2^{DL488} onto OS(+) dECM previously treated with EDTA, revealed a signal distribution of BMP-2 (Fig. 3Cb) similar to the one obtained from OS(+) dECM loaded with BMP-2^{DL488} and then treated with EDTA (Fig. 3Bf).

The capacity of both OS(-) and OS(+) dECMs to bind and retain BMP-2 was also indirectly assessed by quantifying the unbound BMP-2 using ELISA. The results provided evidence of a non-significantly trend ($p = 0.19$) to higher capacity for OS(+) dECM to bind BMP-2 compared to OS(-) dECM (specifically, 55% and 46%, respectively) (Fig. 4A). Altogether, these data provided evidence that both dECMs sequester exogenous BMP-2 to their matrix but through different, or partly different, sites of interactions. While BMP-2 bound onto the organic components of the OS(-) dECM, it bound onto both the mineral and organic components of the OS(+) dECM.

In order to assess the shelf-life of dECMs containing BMP-2, the bioactivity of BMP-2, either freshly-loaded into the dECMs (fresh conditions) or loaded, freeze-dried, and stored at 4 °C for either 48 h or 11 months, was assessed using pluripotent C2C12 myoblasts seeded on BMP-2-loaded dECMs. The ALP activity mediated by the BMP-2 loaded in the OS(+) dECMs was higher than the one obtained in OS(-) dECMs ($p < 0.05$). In addition, the BMP-2 bioactivity was similar when the complex dECM-BMP-2 was used either freshly prepared or stored for 48 h (Fig. 4B); the signal, however, decreased (−1.2 to −1.3-fold) after storage for 11 months (Fig. 4C). Of note, in the absence of BMP-2, no significant ALP activity from C2C12 cells cultured on both 2D-dECMs was detected (data not shown). Altogether, these results provided evidence that the BMP-2-loaded dECMs remained bioactive even after they had been freeze-dried and stored for short term without significant loss of the BMP-2 bioactivity.

Osteoinductive performance of the BMP-2 loaded-3D-PCL-dECM scaffolds in vivo

In order to determine the osteoinductive potential of the BMP-2-containing dECMs, these matrices were prepared as a surface coating onto 3D PCL scaffolds. To this aim, hMSCs were cultured directly onto the scaffolds for 3 weeks. The adhesion and spreading of Luc-ZsGreen-labelled-MSC onto the PCL fiber surfaces were confirmed by fluorescent microscopy (Fig. 5A). In addition, under standard culture conditions, the cells proliferated over the 3 week-period of culture with a proliferative doubling time of 6.5 days. (Fig. 5B). The ECM deposition onto the fibers of the 3D scaffolds was confirmed by fibrillar collagen and GAG stainings and, both of which looked stronger in OS(-) dECM PCL scaffolds than in OS(+) dECM PCL scaffolds (Fig. 5C). These observations were confirmed by the quantifications of the contents of total protein, fibrillar collagen, and GAGs in scaffolds: OS(+) dECMs contained 2.5-fold less total protein, 2.5-fold less fibrillar

collagen and similar amount of GAGs compared to OS(-) dECMs. In fact, these results with 3D-dECMs were similar to those obtained with 2D-dECMs. It is worthy to note that the stainings were non-homogeneous in both types of scaffolds tested; some areas (especially in the periphery of the scaffolds) were weakly stained, while the scaffold centers were darker indicating a non-homogeneous cell distribution and proliferation within the PCL scaffolds. SEM observation of 3D scaffolds confirmed the presence of numerous matrix fibers anchored around, and crossing, the scaffold PCL fibers (Fig. 5E). The presence of CaP crystals within the OS(+) 3D-PCL-dECMs was confirmed both by SEM (Fig. 5E) and by the alizarin red staining (Fig. 5F).

Quantification of fluorescence emitted by BMP-2^{DL800}-loaded within the 3D-PCL scaffolds showed a significant higher capacity of OS(+) dECMs to bind BMP-2 compared to OS(-) dECMs; these OS(+) and OS(-) dECMs bound 1.6- and 1.2-fold higher amounts of BMP-2^{DL800}, respectively, than the bare scaffolds (Fig. 7A).

These BMP-2 loaded scaffolds were implanted ectopically in nude mice and, the new bone formation was monitored using µ-CT analysis during 8-weeks post-implantation. The radiolucent feature of PCL facilitated observation and subsequent quantification of the bone tissue (Fig. 6A). New bone was detected as early as 2-weeks post-implantation and remained constant during the 8-weeks post-implantation in both the BMP-2-containing OS(-) and OS(+) 3D-PCL-dECM scaffolds. The new bone deposited at the periphery of the disk-shaped scaffolds and around the PCL fibers (Fig. 6A). In contrast, the bare 3D-PCL scaffolds loaded with BMP-2 induced either none or minimal new bone formation.

Quantification of the new bone using µCT-analysis confirmed significantly ($p< 0.05$) higher (2.15-, 1.90- and 1.65- fold at week 2, 4 and 8 post-implantation, respectively) new bone formation when the BMP-2 was loaded in the OS(+) 3D-PCL-dECM compared to results obtained when the BMP-2 was loaded in OS(-) 3D-PCL-dECM (Fig. 6B). In addition, in the absence of BMP-2, both dECM-coated 3D-PCL scaffolds tested did not promote bone formation (Fig. 6B) proving that these matrices were not osteoinductive per se. Histologic examination of the explants confirmed that bare PCL scaffolds with adsorbed BMP-2 did not promote noticeable new bone formation (Fig. 6C). In contrast, woven bone was present both on the surfaces and in-between the PCL fibers within the 3D-PCL-dECM scaffolds. Noticeably, new bone was observed only at the periphery of OS(-) 3D-PCL-dECM scaffolds, but was found both around and within the center of all OS(+) 3D-PCL-dECM scaffolds (Fig. 6C-D). Such bone tissue contained embedded osteocytes and osteoblasts laying down osteoid tissue, which is consistent with active new bone formation. In addition, the new bone tissue was surrounded by vascularized marrow spaces containing adipose tissue (Fig. 6D).

Kinetic analysis of BMP-2^{DL800} remaining within the 3D-PCL scaffolds in vivo using fluorescence imaging provided evidence that all scaffolds released BMP-2^{DL800} for at least 2 weeks post-implantation (Fig. 7B-C). Both the bare 3D-PCL and OS(-) 3D-PCL-dECM scaffolds, however, exhibited faster release of BMP-2^{DL800} than that obtained from the OS(+) 3D-PCL-dECM scaffolds. The pharmacokinetics parameters, including AUC, MRT and half-lives, were all higher in OS(+) 3D-PCL-dECM scaffolds, while similar values were observed for the OS(-) 3D-PCL-dECM and bare scaffolds (Fig. 7D). Twenty-two days after implantation, more than 95% of the loaded BMP-2^{DL800} had been released from all scaffolds tested.

The mineral components in OS(+) dECMs were not critical for the matrix efficacy as BMP-2 carrier

Compared to OS(-) dECM, an important feature of the OS(+) dECM is the presence of CaP crystals within the matrix. The BMP-2 protein bound onto both the mineral and organic components of the OS(+) dECM (Fig. 3); for this reason, the contribution of CaP crystals to the higher observed osteoinductivity of these calcified matrices when combined with BMP-2 was determined. For this purpose, the OS(+) dECMs were decalcified using EDTA, rinsed with PBS and then loaded with BMP-2; the bioactivity of these BMP-2-containing matrices was then determined both in vitro and in vivo. The ALP activity of C2C12 cells seeded on EDTA-treated OS(+) 2D-dECM was similar to the one obtained on untreated OS(+) 2D-dECM (Fig. 8A). In addition, the amount of new bone formed in both EDTA-treated-OS(+) and OS(+) 3D-PCL-dECM scaffolds containing BMP-2 were also similar at both 2 and 8 weeks post-implantation (Fig. 8B). These data provided evidence that the CaP minerals contained in the OS(+) dECMs, although retaining 60–80% of the loaded BMP-2, were not critical contributors to the osteoinductive efficacy of these matrices combined with BMP-2.

Discussion

In the present study, we assessed and compared the efficacy of decellularized ECMs derived from osteogenic-differentiated and undifferentiated hMSCs as BMP-2 delivery system both in vitro and in vivo. Our results provided evidence that both dECMs bind BMP-2 and promote bone formation when implanted ectopically in mice. The osteoinductive potential of BMP-2 was, however, higher when loaded within an osteogenic MSC-derived dECM (Os(+) dECM); this outcome was correlated with greater sequestration and retention capacities of BMP-2 over time in vivo. Interestingly, the organic components, but not the CaP minerals contained in these osteogenic matrices, were the critical components for the matrix efficacy as BMP-2 carrier.

Because ECM confers a microenvironment instructive for the regulation of several cellular functions, ECMs derived from in vitro cultured cells have been emerging as promising biological materials for various tissue engineering and regenerative medicine applications. In the skeletal tissue engineering field, cell-derived ECMs are mainly investigated as scaffold-coatings to improve the biological activity and tissue integration of synthetic material scaffolds (see [35] for review). Despite the natural affinities of ECM-derived compounds for growth factors such as BMPs, to date, few studies have examined the use of cultured cell-derived ECM for sustained release of BMP-2. Kang et al. [24] reported that in vitro hMSC-derived ECM deposited on CaP scaffolds bound, and significantly slowed the release of BMP-2 compared to results obtained from uncoated scaffolds; in addition, Kwon et al. [25] demonstrated that rat osteoblast-derived ECM supplemented with BMP-2 promoted the osteogenic commitment of hMSCs in vitro; these studies, however, had no in vivo evaluations. More recently, Kim et al. [36] developed a PLGA/PLA mesh-scaffold coated with a fibroblast-derived ECM capable of immobilizing, and releasing in a controlled manner, BMP-2 which had been immobilized via heparin covalently linked, and not naturally physisorbed, onto the ECM; this study reported improved healing of a rat calvarial bone defect.

In the present study, bone marrow-derived hMSCs were chosen and used to prepare the dECMs tested because of the ability

of these cells to deposit ECM that mimics that of bone tissue; the hMSCs were cultured either under standard cell culture medium or under osteogenic cell culture medium to produce ECM as coating on material surfaces (either on 2D tissue culture polystyrene plastic or on 3D-PCL scaffold). Review of the literature showed that two main methods are used to produce decellularized ECMs from cultured MSCs: exposure either to non-ionic detergents or to chelating agents [22]. In the present study, the chelating decellularization method was excluded in order to maintain the presence of the CaP crystals contained within the OS(+) dECM and, the chemical process (using alkaline reagent and detergent) was used. It is an established method to efficiently remove cellular components (including DNA) [37] that may subsequently cause adverse immune reactions. It is worthy to note, however, that 17–26% of DNA remained in the dECMs after this process; an additional treatment of dECMs with DNase would have improved the rate of DNA elimination. dECMs of different composition and structure were synthesized following these preparation conditions. As both 2D and 3D coatings, the OS (+) dECMs enclosed numerous CaP crystals and, conversely, contained less core ECM constituents, i.e., less proteins (including fibrillary collagens), and displayed a matrix structure with more widely spaced and thicker fibers compared to results obtained with OS(-) dECMs.

Compared to OS(-) dECMs, a non-significant trend of higher capacity for OS(+) dECMs to bind BMP-2 was determined in 2D conditions (Fig. 4A); such trend, however, became significantly different when comparing dECMs coated onto 3D-PCL scaffolds (Fig. 7A); the higher coating surface in 3D-PCL scaffolds compared to 2D-plastic wells may explain this difference. The in vitro BMP-2 bioactivity (assessed using pluripotent C2C12 myoblasts) was also higher on OS(+) dECM. Promisingly, the BMP-2 contained in both dECMs (that had been air-dried and stored at 4 °C) remained bioactive for at least 11 months; no significant loss of BMP-2 bioactivity was observed 48 h after the freeze-drying / storage process while there was ~25–30% of decrease after 11 months of storage. It is, therefore, the long-term storage rather than the freeze-drying process that affects the BMP-2 bioactivity overtime. This information regarding the shelf-life of BMP-2 immobilized onto material surfaces is critical for subsequent clinical availability and use.

The observed ectopic bone formation in mice induced by the BMP-2 contained in dECM-coated 3D-PCL scaffolds confirmed the osteoinductive performance of the coated implants tested. Mineralized bone tissue was produced through a direct apposition process mainly localized at the surface of the dECM-coated PCL fibers. Bone quantification by µ-CT indicated higher bone formation within the OS(+) dECM-coated 3D-PCL scaffolds compared to the OS(-) dECM-coated 3D-PCL scaffolds. In addition, histological examination of explants after 8 weeks post-implantation revealed a more homogeneous distribution of bone tissue (especially, the presence of bone tissue within the center of the scaffold) within the OS(+) dECM-coated 3D-PCL scaffolds. This result can be explained by the differences in dECM distribution and composition; for instance the presence of CaP mineral crystals in OS(+) dECMs may render these matrices more osteoconductive compared to OS(-) ECMs. It could be also linked to the higher level of BMP-2 retention of OS(+) compared to OS(-) dECMs since this pleiotropic growth factor has numerous dose-dependent functions including ones with proliferative, chemoattractive, differentiative and angiogenetic properties [38]. These overall data provided evidence of the superiority of OS(+) dECM as BMP-2 carrier to promote new bone formation. It is noteworthy that the kinetics of bone formation was very fast for both dECM tested with a plateau reached 2 weeks after implantation. This fast osteogenesis outcome is in agreement with literature reports or studies that used surface coatings of materials with poly (L-lysine) / hyaluronic acid polyelectrolyte films to deliver BMP-2, and showed a fast (1–2 weeks) healing of a femoral bone defect in rats [39].

In order to facilitate the in vivo quantification of bound and retained BMP-2 in situ within the 3D-dECMs over time, the protein was labelled with a Dylight NIR fluorophore known for its brightness and photo-stability; NIR light can also penetrate deeper into tissue and causes less photodamage to cells compared to UV/visible light [40]. Based on the fluorescence emitted from the BMP-2^{DL800}-loaded 3D-PCL scaffolds, the BMP-2 dose delivered in vivo in the present study was estimated to be ~2.6, 2.0 and 1.6 µg in implants coated with OS(+) dECM-coated, OS(-) dECM-coated and in bare 3D-PCL scaffolds, respectively. It is known that BMP-2 promotes bone formation in a dose-dependent manner [41]; the higher amount of newly-formed bone in OS(+) dECM 3D-PCL scaffolds, therefore, can be explained by the higher dose of BMP-2 contained in these implants. Another key point for optimal bone regeneration mediated by BMP-2 is the efficacy of the carrier to control the release kinetics of the protein [42]. Most reported studies focused on the delivery of BMP-2 from biomaterials estimated its release in vitro, in buffers that do not utterly mimic the in vivo physiological environment; these in vitro models, therefore, were not dependable predictors for in vivo release of BMP-2 [43]. For this reason, we monitored in vivo, non-invasively, the amount of remained BMP-2^{DL800} within each 3D-PCL scaffold tested. The release kinetics demonstrated that the OS(+) dECM 3D-PCL scaffolds retained more efficiently the BMP-2 over the duration of the implantation, with a mean retention time and half-life of BMP-2, 1.3- and 2.5-fold higher, respectively, than in the OS(-) dECM 3D-PCL scaffolds. Although the optimized release profile of BMP-2 for enhanced bone regeneration still remains a challenge, review of the literature provided evidence that long-term delivery of BMP-2 enhances the in vivo osteogenic efficacy of the protein compared to short-term delivery at an equivalent dose [42,44,45]. Altogether, the results of the present study provided evidence that, compared to the non-osteogenic OS(-) dECM, the osteogenic OS(+) dECM was an effective carrier of BMP-2 due to its capability to bind the protein and retain it in situ more efficiently over the two first weeks post-implantation.

It is noteworthy that the bare 3D-PCL scaffolds, contained only 17% less of BMP-2 than the OS(-) dECM 3D-PCL scaffolds at the time of implantation and exhibited a similar release kinetics of BMP-2, but did not promote significant bone formation compared to the OS(-) dECM 3D-PCL scaffolds. This outcome could be explained by a minimum dose of BMP-2 required in situ to induce new bone formation. Another explanation is the role that the dECM coated onto the 3D-PCL scaffolds may play on tissue regeneration. Such kind of coating may, conceivably, confer bioactivity to inert materials like PCL, and affect the cell fate of host cells. In fact, numerous studies reported in the literature that decellularized matrices derived from various cell types (either fibroblasts [46], MSCs [47,48] or pre-osteoblasts [46,49,50]) modulated the function of cultured MSCs; specifically, MSC-derived ECM either enhanced or maintained the osteogenic differentiation of MSCs [51], [52], [53]. In vivo, material scaffolds

coated with MSC-secreted ECMs and implanted in rodents, promoted vascularization, formation of a mineralized matrix [48,53], and healing of bone defects [54]; these studies, however, failed to demonstrate induction of bone formation ectopically, suggesting the absence of a clear osteoinductive potential of these matrices. In the present study, the in vitro results confirmed the beneficial effects of the dECMs on hMSCs functions. Both dECM promoted adhesion and proliferation of cultured hMSCs; the OS(+) dECM, however, better promoted hMSC proliferation, while the OS(-) dECM better promoted hMSC osteogenic differentiation. In addition, in vivo, the dECM-coated 3D-PCL scaffolds did not promote bone formation in the absence of BMP-2 proving that these matrices were not osteoinductive *per se*.

In order to identify the matrix components responsible for the higher capacity of OS(+) dECM to bind and retain BMP-2, we determined the localization of the protein bound within the dECMs. Our data showed that BMP-2 bound on both dECMs but at different sites. In fact, as BMP-2 bound onto the organic components of the OS(-) dECM, a large part of the growth factor bound onto the CaP crystals contained within the OS(+) dECM. Literature reports demonstrated the adsorption of BMP-2 on apatitic calcium phosphate (including tricalcium phosphate and hydroxyapatite) conferring osteoinductive properties to these ceramics [26,27]. Further analysis of the adsorption process of BMP-2 on CaP surfaces provided evidence of both electrostatic and H-bonding between the Ca^{2+} and PO_4^{3-} ions from the ceramics and the COO^-, NH_2 and OH residues of the protein, [28,55,56].

The present study also determined whether the CaP crystals contained within the OS(+) dECMs were responsible for their higher osteoinductivity when combined with BMP-2. Pre-treatment of the OS(+) dECMs with EDTA (to eliminate the CaP crystals) did not affect the bioactivities of BMP-2 loaded in these dECMS, both in vitro and in vivo (Fig. 7). It is worthy to note that the in vitro bioactivity of BMP-2 contained in 2D-dECM deposited by hMSCs cultured in osteogenic medium without β-glycerophosphate (that serves mainly as a source of inorganic phosphate for matrix mineralization) was also tested and no difference with OS(+) dECMs-contained BMP-2 was observed (data not shown). One may conclude that the CaP minerals contained in these osteogenic matrices were not critical components for the dECM efficacy as BMP-2 carrier, and, conversely, the organic components, even though present in a lower amount than in the OS(-) dECMs, represent the critical components. In vitro fluorescent imaging of BMP-2 onto the decalcified (EDTA treated) OS(+) dECMs indicated that, in addition to the CaP crystals, BMP-2 bound to the organic components of the ECM (Fig. 3B). In the present study, the composition of the dECMs were not analyzed in detail and, therefore, the pertinent components involved in the higher efficacy of OS(+) dECM to sequester and promote the activity of BMP-2 were not identified. The review of the literature gives some information on the MSC-derived matrices compositions. For instance, using mass spectroscopy analysis, Thibault et al. showed that rat bone marrow-derived MSCs, cultured under osteogenic conditions, deposited cellular adhesion proteins, such as fibronectin, at short culture durations while they deposited matrix remodeling and regulatory proteins, such as MMP-2 and PEDF, at long culture durations [57]. Kim et al. found that the levels of cytoskeleton-organizing proteins, morphogenesis-related proteins, and calcium-binding proteins increased in human bone marrow-derived MSCs during osteogenesis [58]. More recently, Shaik et al. analyzed the transcriptome profile of osteogenic induced adipose tissue-derived hMSC in comparison with undifferentiated cells and found that 35% of glycoproteins, 22% of collagens and proteoglycans, 41% of ECM-affiliated regulators, 29% of regulators, and 50% of secreted factors were upregulated during osteogenesis [59].

Regarding the BMP-2 binding-ECM components, it is well-known that BMP-2, via an N-terminal heparin binding region, interacts directly with GAGs [14]. Other literature reports demonstrated the high affinity of the BMP-2 protein with various ECM components such as fibronectin, tenascin C, osteopontin [15], which were also shown to be expressed during osteogenesis [50,60]. In the present study, the OS(+) and OS(-) dECMs tested differ not only in their content of components that constitute the core matrisome (i.e., collagens, glycoproteins and proteoglycans) but also likely in their matrisome-associated proteins (i.e., regulators, secreted factors, and other ECM-affiliated proteins). Recently, Onishi et al. [54] showed the presence of growth factors including BMP-2, VEGF, bFGF and TGF-β1 in dECM derived from hMSC; these growth factors, which are involved in the process of new bone formation, were preserved after decellularization by freeze-thawing. In the present study, the chemical decellularization process used, however, may have removed some of the signaling molecules. Undoubtedly, differences in ECM composition, including both core matrisome macromolecules and matrisome-associated proteins, may explain the advantage of OS(+) dECM as an effective BMP-2 carrier.

In the present study, we applied MSC-derived ECMs as coating of 3D scaffolds of PCL, a long-term (from 1 to 3 years) biodegradable polymer that has been approved for use as a bone graft substitute [62]. Such approach aims to improve the functionality and tissue integration of synthetic material scaffolds of different shapes and chemical nature that do not have a natural affinity for the growth factor [61]. Our results provided evidence that the coating of PCL implants with BMP-2-loaded dECM conferred the implant surface with osteoinductive properties, promoting a fast and local bone formation activity. This approach differs from using a space-filling material such as collagen sponge (the current clinical standard scaffold) or hydrogel in which the growth factor is physically entrapped, and released as a function of various parameters such as macromolecule mesh size, viscosity of the liquid phase and spatiotemporal degradation profile of the scaffold [63]. Of note, additional experiments (data not shown) confirmed the efficacy of collagen sponge as BMP-2 carrier to induce bone tissue ectopically but with a slower bone formation kinetics than obtained with 3D-PCL-dECMs; when loaded with similar dose of BMP-2, the osteoinductivity of collagen sponge remained lower than the one obtained with OS(+) dECM. The performance of both scaffold coatings and sponges as BMP-2 carriers, however, cannot be compared, because of the different macro- and micro-architecture of both carriers as well as the different physico-chemical mechanisms of the growth factor delivery. Preparation of dECMs as sponge or cell sheets without scaffold, however, is achievable through lifting of the cell layer and, possibly, crosslinking [54]. As a result, cell-derived osteogenic ECMs, either as scaffold coatings or as sponge/cell sheets, represent promising BMP-2 carriers for bone tissue engineering.

Conclusion

We demonstrated that a decellularized ECM produced by hMSCs, that can coat a wide variety of materials, can be used as a delivery platform for BMP-2. The dECMs tested in the present study bind and maintain bioactive BMP-2 even after lyophilization, a prerequisite for protein storage. More interestingly, compared to dECMs prepared with undifferentiated hMSCs, the dECMs derived from osteogenic differentiated hMSCs loaded with BMP-2 were more effective in promoting ectopic bone formation in mice. This higher osteoinductive potential was correlated with greater capacities of BMP-2 sequestration and maintenance post-implantation. Although the BMP-2 mainly bound onto the CaP crystals contained within the osteogenic dECM, these mineral components were not involved in the observed higher osteoinductivity, suggesting that the organic components were the critical matrix components for the OS(+) dECM efficacy as BMP-2 carriers.

Author contributions

NL: Conceptualization; Investigation; Methodology; Writing-Original Draft; **HE-H**: Methodology; Investigation; **EP**: Formal Analysis; Validation; Review and Editing; **NS**: Methodology; Validation; Visualization; **MB**: Methodology; Investigation and Visualization; **HP**: Conceptualization and Supervision; Review and Editing; Funding Acquisition; **DL-A**: Conceptualization, Supervision and Administration; Writing-Reviewing and Editing; Funding Acquisition.

Acknowledgments

The authors thank Medtronic Inc. for kindly providing BMP-2, Prof. R. Bizios for reviewing the manuscript, F. Pillier (UPR15-CNRS LISE) for SEM-EDX analyses and the Vect'UB vectorology facility (TBMCore, Bordeaux) for Lentiviral production. This study was supported by the center National de la Recherche Scientifique (CNRS).

Declaration of Competing Interest

The authors declare that they have no known competing financial interests or personal relationships that could have appeared to influence the work reported in this paper.

References

[1] P.V. Giannoudis, T.A. Einhorn, D. Marsh. Fracture healing: the diamond concept. Injury, 38 (2007), pp. S3-S6, 10.1016/S0020-1383(08)70003-2

[2] K. Tsuji, A. Bandyopadhyay, B.D. Harfe, K. Cox, S. Kakar, L. Gerstenfeld, T. Einhorn, C.J. Tabin, V. Rosen, B.M.P.2. activity although dispensable for bone formation, is required for the initiation of fracture healing. Nat. Genet., 38 (2006), pp. 1424-1429, 10.1038/ng1916

[3] V. Rosen. BMP2 signaling in bone development and repair. Cytokine Growth Factor Rev., 20 (2009), pp. 475-480, 10.1016/j.cytogfr.2009.10.018

[4] Y.Y. Yu, S. Lieu, C. Lu, T. Miclau, R.S. Marcucio, C. Colnot. Immunolocalization of BMPs, BMP antagonists, receptors, and effectors during fracture repair. Bone, 46 (2010), pp. 841-851, 10.1016/j.bone.2009.11.005

[5] J.K. Burkus, M.F. Gornet, C.A. Dickman, T.A. Zdeblick. Anterior lumbar interbody fusion using rhBMP-2 with tapered interbody cages. J. Spinal. Disord. Tech., 15 (2002), pp. 337-349

[6] S. Govender, C. Csimma, H.K. Genant, A. Valentin-Opran, Y. Amit, R. Arbel, H. Aro, D. Atar, M. Bishay, M.G. Börner, P. Chiron, P. Choong, J. Cinats, B. Courtenay, R. Feibel, B. Geulette, C. Gravel, N. Haas, M. Raschke, E. Hammacher, D. van der Velde, P. Hardy, M. Holt, C. Josten, R.L. Ketterl, B. Lindeque, G. Lob, H. Mathevon, G. McCoy, D. Marsh, R. Miller, E. Munting, S. Oevre, L. Nordsletten, A. Patel, A. Pohl, W. Rennie, P. Reynders, P.M. Rommens, J. Rondia, W.C. Rossouw, P.J. Daneel, S. Ruff, A. Rüter, S. Santavirta, T.A. Schildhauer, C. Gekle, R. Schnettler, D. Segal, H. Seiler, R.B. Snowdowne, J. Stapert, G. Taglang, R. Verdonk, L. Vogels, A. Weckbach, A. Wentzensen, T. Wisniewski. BMP-2 Evaluation in Surgery for Tibial Trauma (BESTT) Study Group, Recombinant human bone morphogenetic protein-2 for treatment of open tibial fractures: a prospective, controlled, randomized study of four hundred and fifty patients. J. Bone Joint Surg. Am., 84-A (2002), pp. 2123-2134

[7] J.N. Zara, R.K. Siu, X. Zhang, J. Shen, R. Ngo, M. Lee, W. Li, M. Chiang, J. Chung, J. Kwak, B.M. Wu, K. Ting, C. Soo. High doses of bone morphogenetic protein 2 induce structurally abnormal bone and inflammation In Vivo. Tissue Eng. Part A, 17 (2011), pp. 1389-1399, 10.1089/ten.tea.2010.0555

[8] J.K. Burkus, H.S. Sandhu, M.F. Gornet. Influence of rhBMP-2 on the healing patterns associated with allograft interbody constructs in comparison with autograft. Spine, 31 (2006), pp. 775-781, 10.1097/01.brs.0000206357.88287.5a

[9] J.W. McClellan, D.S. Mulconrey, R.J. Forbes, N. Fullmer. Vertebral bone resorption after transforaminal lumbar interbody fusion with bone morphogenetic protein (rhBMP-2). J. Spinal Disord. Tech., 19 (2006), pp. 483-486, 10.1097/01.bsd.0000211231.83716.4b

[10] E.J. Carragee, E.L. Hurwitz, B.K. Weiner. A critical review of recombinant human bone morphogenetic protein-2 trials in spinal surgery: emerging safety concerns and lessons learned. Spine J., 11 (2011), pp. 471-491, 10.1016/j.spinee.2011.04.023

[11] A.W. James, G. LaChaud, J. Shen, G. Asatrian, V. Nguyen, X. Zhang, K. Ting, C. Soo. A review of the clinical side effects of bone morphogenetic protein-2. Tissue Eng. Part B, 22 (2016), pp. 284-297, 10.1089/ten.teb.2015.0357

[12] H. Huang, D. Wismeijer, E. Hunziker, G. Wu. The acute inflammatory response to absorbed collagen sponge is not enhanced by BMP-2. Int. J. Mol. Sci., 18 (2017), p. 498, 10.3390/ijms18030498

[13] V. Agrawal, M. Sinha. A review on carrier systems for bone morphogenetic protein-2: review on BMP-2 Carrier System. J. Biomed. Mater. Res., 105 (2017), pp. 904-925, 10.1002/jbm.b.33599

[14] R. Ruppert, E. Hoffmann, W. Sebald. Human bone morphogenetic protein 2 contains a heparin-binding site which modifies its biological activity. Eur. J. Biochem., 237 (1996), pp. 295-302, 10.1111/j.1432-1033.1996.0295n.x

[15] M.M. Martino, P.S. Briquez, E. Guc, F. Tortelli, W.W. Kilarski, S. Metzger, J.J. Rice, G.A. Kuhn, R. Muller, M.A. Swartz, J.A. Hubbell. Growth factors engineered for super-affinity to the extracellular matrix enhance tissue healing. Science, 343 (2014), pp. 885-888, 10.1126/science.1247663

[16] A.P. Wohl, H. Troilo, R.F. Collins, C. Baldock, G. Sengle. Extracellular regulation of bone morphogenetic protein activity by the microfibril component fibrillin-1. J. Biol. Chem., 291 (2016), pp. 12732-12746, 10.1074/jbc.M115.704734

[17] F.P. Seib, B. Lanfer, M. Bornhäuser, C. Werner. Biological activity of extracellular matrix-associated BMP-2. J Tissue Eng Regen Med, 4 (2009), pp. 324-327, 10.1002/term.240

[18] G. Sanchez-Duffhues, C. Hiepen, P. Knaus, P.ten Dijke. Bone morphogenetic protein signaling in bone homeostasis. Bone, 80 (2015), pp. 43-59, 10.1016/j.bone.2015.05.025

[19] M. Kisiel, A.S. Klar, M. Ventura, J. Buijs, M.-.K. Mafina, S.M. Cool, J. Hilborn. Complexation and sequestration of BMP-2 from an ECM mimetic hyaluronan Gel for improved bone formation. PLoS ONE, 8 (2013), p. e78551, 10.1371/journal.pone.0078551

[20] T. Boudou, T. Crouzier, K. Ren, G. Blin, C. Picart. Multiple functionalities of polyelectrolyte multilayer films: new biomedical applications. Adv. Mater. Weinheim, 22 (2010), pp. 441-467, 10.1002/adma.200901327

[21] B. Antebi, Z. Zhang, Y. Wang, Z. Lu, X.-.D. Chen, J. Ling. Stromal-cell-derived extracellular matrix promotes the proliferation and retains the osteogenic differentiation capacity of mesenchymal stem cells

on three-dimensional scaffolds. Tissue Eng. Part C, 21 (2015), pp. 171-181, 10.1089/ten.tec.2014.0092

[22] A. Shakouri-Motlagh, A.J. O'Connor, S.P. Brennecke, B. Kalionis, D.E. Heath. Native and solubilized decellularized extracellular matrix: a critical assessment of their potential for improving the expansion of mesenchymal stem cells. Acta Biomater, 55 (2017), pp. 1-12, 10.1016/j.actbio.2017.04.014

[23] M. Grünert, C. Dombrowski, M. Sadasivam, K. Manton, S.M. Cool, V. Nurcombe. Isolation of a native osteoblast matrix with a specific affinity for BMP2. J. Mol. Histol., 38 (2007), pp. 393-404, 10.1007/s10735-007-9119-0

[24] Y. Kang, S. Kim, A. Khademhosseini, Y. Yang. Creation of bony microenvironment with CaP and cell-derived ECM to enhance human bone-marrow MSC behavior and delivery of BMP-2. Biomaterials, 32 (2011), pp. 6119-6130, 10.1016/j.biomaterials.2011.05.015

[25] S.-.H. Kwon, T.-.J. Lee, J. Park, J.-.E. Hwang, M. Jin, H.-.K. Jang, N.S. Hwang, B.-.S. Kim. Modulation of BMP-2-induced chondrogenic versus osteogenic differentiation of human mesenchymal stem cells by cell-specific extracellular matrices. Tissue Eng. Part A, 19 (2013), pp. 49-58, 10.1089/ten.tea.2012.0245

[26] M.R. Urist, A. Lietze, E. Dawson. Beta-tricalcium phosphate delivery system for bone morphogenetic protein. Clin. Orthop. Relat. Res (1984), pp. 277-280

[27] I. Alam, I. Asahina, K. Ohmamiuda, K. Takahashi, S. Yokota, S. Enomoto. Evaluation of ceramics composed of different hydroxyapatite to tricalcium phosphate ratios as carriers for rhBMP-2. Biomaterials, 22 (2001), pp. 1643-1651, 10.1016/S0142-9612(00)00322-7

[28] T. Boix, J. Gómez-Morales, J. Torrent-Burgués, A. Monfort, P. Puigdomènech, R. Rodríguez-Clemente. Adsorption of recombinant human bone morphogenetic protein rhBMP-2m onto hydroxyapatite. J. Inorg. Biochem., 99 (2005), pp. 1043-1050, 10.1016/j.jinorgbio.2005.01.011

[29] A. Moya, N. Larochette, M. Bourguignon, H. El-Hafci, E. Potier, H. Petite, D. Logeart-Avramoglou. Osteogenic potential of adipogenic predifferentiated human bone marrow-derived multipotent stromal cells for bone tissue-engineering. J. Tissue Eng. Regen. Med., 12 (2018), pp. e1511-e1524, 10.1002/term.2571

[30] P. Becquart, A. Cambon-Binder, L.-.E. Monfoulet, M. Bourguignon, K. Vandamme, M. Bensidhoum, H. Petite, D. Logeart-Avramoglou. Ischemia is the prime but not the only cause of human multipotent stromal cell death in tissue-engineered constructs In Vivo. Tissue Eng. Part A, 18 (2012), pp. 2084-2094, 10.1089/ten.tea.2011.0690

[31] A. Lopez-De Leon, M. Rojkind. A simple micromethod for collagen and total protein determination in formalin-fixed paraffin-embedded sections. J. Histochem. Cytochem., 33 (1985), pp. 737-743, 10.1177/33.8.2410480

[32] L.-.E. Monfoulet, P. Becquart, D. Marchat, K. Vandamme, M. Bourguignon, E. Pacard, V. Viateau, H. Petite, D. Logeart-Avramoglou. The pH in the microenvironment of human mesenchymal stem cells is a critical factor for optimal osteogenesis in tissue-engineered constructs. Tissue Eng. Part A, 20 (2014), pp. 1827-1840, 10.1089/ten.tea.2013.0500

[33] T. Katagiri, A. Yamaguchi, M. Komaki, E. Abe, N. Takahashi, T. Ikeda, V. Rosen, J.M. Wozney, A. Fujisawa-Sehara, T. Suda. Bone morphogenetic protein-2 converts the differentiation pathway of C2C12 myoblasts into the osteoblast lineage. J. Cell Biol, 127 (1994), pp. 1755-1766

[34] N. Otsu. A threshold selection method from gray-level histograms. IEEE Trans. Syst., Man, Cybern, 9 (1979), pp. 62-66, 10.1109/TSMC.1979.4310076

[35] L.E. Fitzpatrick, T.C. McDevitt. Cell-derived matrices for tissue engineering and regenerative medicine applications. Biomater Sci, 3 (2015), pp. 12-24, 10.1039/C4BM00246F

[36] I.G. Kim, M.P. Hwang, P. Du, J. Ko, C. Ha, S.H. Do, K. Park. Bioactive cell-derived matrices combined with polymer mesh scaffold for osteogenesis and bone healing. Biomaterials, 50 (2015), pp. 75-86, 10.1016/j.biomaterials.2015.01.054

[37] S. Badylak, D. Freytes, T. Gilbert. Extracellular matrix as a biological scaffold material: structure and function. Acta Biomater, 5 (2009), pp. 1-13, 10.1016/j.actbio.2008.09.013

[38] G. Finkenzeller, S. Hager, G.B. Stark. Effects of bone morphogenetic protein 2 on human umbilical vein endothelial cells. Microvasc. Res, 84 (2012), pp. 81-85, 10.1016/j.mvr.2012.03.010

[39] M. Bouyer, R. Guillot, J. Lavaud, C. Plettinx, C. Olivier, V. Curry, J. Boutonnat, J.-.L. Coll, F. Peyrin, V. Josserand, G. Bettega, C. Picart. Surface delivery of tunable doses of BMP-2 from an adaptable polymeric scaffold induces volumetric bone regeneration. Biomaterials, 104 (2016), pp. 168-181, 10.1016/j.biomaterials.2016.06.001

[40] A. Douplik, G. Saiko, I. Schelkanova, V.V. Tuchin. The response of tissue to laser light, in: lasers for medical applications. Elsevier (2013), pp. 47-109, 10.1533/9780857097545.1.47

[41] E.A. Wang, V. Rosen, J.S. D'Alessandro, M. Bauduy, P. Cordes, T. Harada, D.I. Israel, R.M. Hewick, K.M. Kerns, P. LaPan. Recombinant human bone morphogenetic protein induces bone formation. Proceedings of the National Academy of Sciences, 87 (1990), pp. 2220-2224

[42] T.-.M. De Witte, L.E. Fratila-Apachitei, A.A. Zadpoor, N.A. Peppas. Bone tissue engineering via growth factor delivery: from scaffolds to complex matrices. Regen. Biomater, 5 (2018), pp. 197-211, 10.1093/rb/rby013

[43] M.G.L. Olthof, M.A. Tryfonidou, M. Dadsetan, W.J.A. Dhert, M.J. Yaszemski, D.H.R. Kempen, L. Lu. In Vitro and In Vivo correlation of bone morphogenetic protein-2 release profiles from complex delivery vehicles. Tissue Eng. Part C, 24 (2018), pp. 379-390, 10.1089/ten.tec.2018.0024

[44] H. Uludag, D. D'Augusta, J. Golden, J. Li, G. Timony, R. Riedel, J.M. Wozney. Implantation of recombinant human bone morphogenetic proteins with biomaterial carriers: a correlation between protein pharmacokinetics and osteoinduction in the rat ectopic model. J. Biomed. Mater. Res., 50 (2000), pp. 227-238, 10.1002/(sici)1097-4636(200005)50

[45] O. Jeon, S.J. Song, H.S. Yang, S.-.H. Bhang, S.-.W. Kang, M.A. Sung, J.H. Lee, B.-.S. Kim. Long-term delivery enhances in vivo osteogenic efficacy of bone morphogenetic protein-2 compared to short-term delivery. Biochem. Biophys. Res. Commun. (2008), p. 7

[46] Y.J. Hong, S.E. Bae, S.H. Do, I.H. Kim, D.K. Han, K. Park. Decellularized PLGA-based scaffolds and their osteogenic potential with bone marrow stromal cells. Macromol. Res, 19 (2011), pp. 1090-1096, 10.1007/s13233-011-1004-8

[47] M.L. Decaris, A. Mojadedi, A. Bhat, J.K. Leach. Transferable cell-secreted extracellular matrices enhance osteogenic differentiation. Acta Biomater, 8 (2012), pp. 744-752, 10.1016/j.actbio.2011.10.035

[48] A.I. Hoch, V. Mittal, D. Mitra, N. Vollmer, C.A. Zikry, J.K. Leach. Cell-secreted matrices perpetuate the bone-forming phenotype of differentiated mesenchymal stem cells. Biomaterials, 74 (2016), pp. 178-187, 10.1016/j.biomaterials.2015.10.003

[49] N. Datta, H.L. Holtorf, V.I. Sikavitsas, J.A. Jansen, A.G. Mikos. Effect of bone extracellular matrix synthesized in vitro on the osteoblastic differentiation of marrow stromal cells. Biomaterials, 26 (2005), pp. 971-977, 10.1016/j.biomaterials.2004.04.001

[50] R.A. Thibault, A.G. Mikos, F.K. Kasper. Osteogenic differentiation of mesenchymal stem cells on demineralized and devitalized biodegradable polymer and extracellular matrix hybrid constructs. J. Biomed. Mater. Res. Part A, 101A (2013), pp. 1225-1236, 10.1002/jbm.a.34610

[51] Q.P. Pham, F. Kurtis Kasper, L. Scott Baggett, R.M. Raphael, J.A. Jansen, A.G. Mikos. The influence of an in vitro generated bone-like extracellular matrix on osteoblastic gene expression of marrow stromal cells. Biomaterials, 29 (2008), pp. 2729-2739, 10.1016/j.biomaterials.2008.02.025

[52] J. Liao, X. Guo, D. Nelson, F. Kurtis Kasper, A.G. Mikos. Modulation of osteogenic properties of biodegradable polymer/extracellular matrix scaffolds generated with a flow perfusion bioreactor. Acta Biomater, 6 (2010), pp. 2386-2393, 10.1016/j.actbio.2010.01.011

[53] N. Sadr, B.E. Pippenger, A. Scherberich, D. Wendt, S. Mantero, I. Martin, A. Papadimitropoulos. Enhancing the biological performance of synthetic polymeric materials by decoration with engineered, decellularized extracellular matrix. Biomaterials, 33 (2012), pp. 5085-5093, 10.1016/j.biomaterials.2012.03.082

[54] T. Onishi, T. Shimizu, M. Akahane, S. Omokawa, A. Okuda, T. Kira, Y. nagak, Y. Tanaka. Osteogenic extracellular matrix sheet for bone

tissue regeneration. Eur. Cell Mater., 36 (2018), pp. 69-80, 10.22203/eCM.v036a06

[55] X. Dong, Q. Wang, T. Wu, H. Pan. Understanding adsorption-desorption dynamics of BMP-2 on hydroxyapatite (001) surface. Biophys. J, 93 (2007), pp. 750-759, 10.1529/biophysj.106.103168

[56] H. Autefage, F. Briand-Mésange, S. Cazalbou, C. Drouet, D. Fourmy, S. Gonçalvès, J.-.P. Salles, C. Combes, P. Swider, C. Rey. Adsorption and release of BMP-2 on nanocrystalline apatite-coated and uncoated hydroxyapatite/beta-tricalcium phosphate porous ceramics. J. Biomed. Mater. Res. Part B Appl. Biomater., 91 (2009), pp. 706-715, 10.1002/jbm.b.31447

[57] R.A. Thibault, A.G. Mikos, F.K. Kasper. Protein and mineral composition of osteogenic extracellular matrix constructs generated with a flow perfusion bioreactor. Biomacromolecules, 12 (2011), pp. 4204-4212, 10.1021/bm200975a

[58] J.-.M. Kim, J. Kim, Y.-.H. Kim, K.-.T. Kim, S.H. Ryu, T.G. Lee, P.-.G. Suh. Comparative secretome analysis of human bone marrow-derived mesenchymal stem cells during osteogenesis. J. Cell. Physiol., 228 (2013), pp. 216-224, 10.1002/jcp.24123

[59] S. Shaik, E.C. Martin, D.J. Hayes, J.M. Gimble, R.V. Devireddy. Transcriptomic profiling of adipose derived stem cells undergoing osteogenesis by RNA-Seq. Sci. Rep, 9 (2019), p. 11800, 10.1038/s41598-019-48089-1

[60] J.M. Morgan, A. Wong, C.E. Yellowley, D.C. Genetos. Regulation of tenascin expression in bone. J. Cell. Biochem., 112 (2011), pp. 3354-3363, 10.1002/jcb.23265

[61] W.J. King, P.H. Krebsbach. Growth factor delivery: how surface interactions modulate release in vitro and in vivo. Adv. Drug Deliv. Rev., 64 (2012), pp. 1239-1256, 10.1016/j.addr.2012.03.004

[62] M. Bartnikowski, T.R. Dargaville, S. Ivanovski, D.W. Hutmacher. Degradation mechanisms of polycaprolactone in the context of chemistry, geometry and environment. Prog. Polym. Sci, 96 (2019), pp. 1-20, 10.1016/j.progpolymsci.2019.05.004

[63] W. Friess. Collagen – biomaterial for drug delivery. Eur. J. Pharmaceut. Biopharmaceut. (1998), p. 24

Corresponding author:
Delphine LOGEART-AVRAMOGLOU
Laboratoire B3OA UMR CNRS 7052 INSERM U1271
Faculté de médecine Université de Paris – Site Villemin
10, Avenue de Verdun
75010 Paris
FRANCE
Email: delphine.logeart@cnrs.fr

Table 1. Experimental groups and analyses performed.

Two groups included BMP-2-free scaffolds and were used as unloaded controls; three groups included scaffolds prepared with either BMP-2 or BMP-2 containing 10% of BMP-2^{DL800} (to monitor the release of the growth factor in vivo by fluorescence imaging). The new bone formation induced by each PCL scaffolds was monitored in vivo using µ-CT at 2, 4 and 8 weeks post-implantation.

Groups	**BMP-2**	**Fluorescence imaging**	**µ-CT**
OS(-) w/o BMP-2	No	NA	N=4
OS(+) w/o BMP-2	No	NA	N=4
Bare with BMP-2	N=3 with BMP-2 N=6 with BMP-2^{DL800}	N=6	N=9
OS(-) with BMP-2	N=6 with BMP-2 N=6 with BMP-2^{DL800}	N=6	N=12
OS(+) with BMP-2	N=6 with BMP-2 N=6 with BMP-2^{DL800}	N=6	N=12

Figure 1. Biochemical characterization of both the ECMs and dECMs.

(A) Protein, fibrillar collagen and GAG contents in both OS(-) and OS(+) matrices before (ECM) and after decellularization (dECM); $n = 5$. (B) SEM images of both OS(-) and OS(+) dECMs. The red arrows indicate the CaP crystals anchored within the matrix fibers. (C) Calcium contents in both OS(-) and OS(+) matrices before (ECM) and after decellularization (dECM); $n = 3$. One-way ANOVA with Tukey's post-hoc test. (a) $p < 0.05$ compared to ECM; (b) $p < 0.05$ compared to OS(-). (For interpretation of the references to colour in this figure legend, the reader is referred to the web version of this article.)

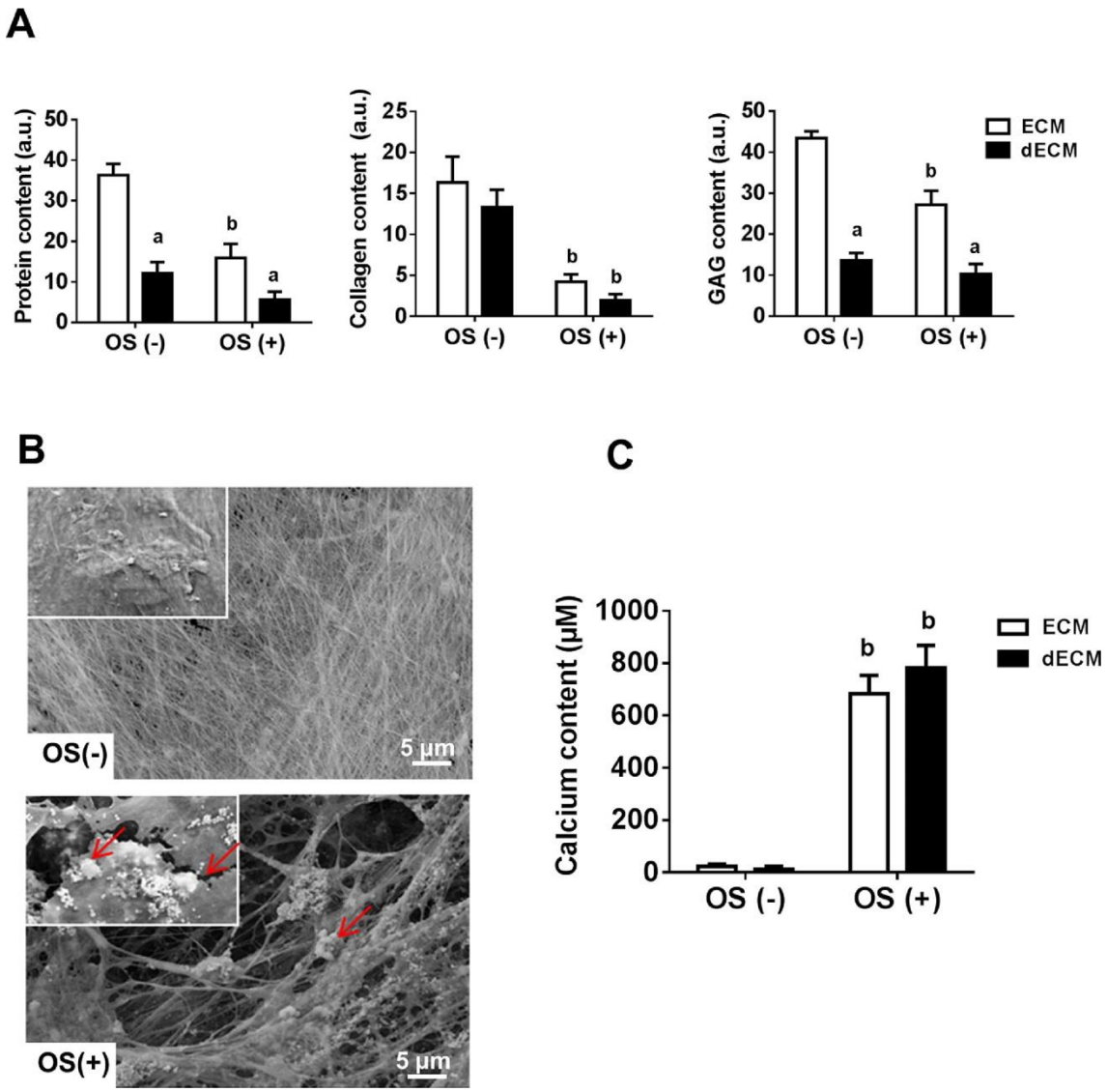

Figure 2. Adhesion, proliferation, and osteogenic differentiation of hMSCs cultured onto either 2D-dECMs or on tissue-culture-plastic substrates (TCP).

(A) Fluorescent microscopy images of hMSC stained with the Cell tracker Orange dye 4 h after cell seeding on each substrate. These images are representative of two separate experiments. (B) Proliferation rate of hMSCs cultured onto each substrate; $n = 3$. (C) Alkaline phosphatase (ALP) activity expressed by hMSCs cultured onto each substrate in either standard (Std) or osteogenic (OG) cell culture medium for 7 days; $n = 3$. (D) Expression of osteogenesis-related genes by hMSCs cultured onto each substrate tested in osteogenic cell culture medium for 14 days; RUNX 2: Runt-related transcription factor 2, ALP: Alkaline phosphatase, and IBSP: integrin binding sialoprotein. Gene expressions were normalized first to that of the respective 18S (internal standard), and then to the respective results obtained for hMSCs at day 0 ($2^{-\Delta\Delta CT}$ format); $n = 3$. One-way ANOVA with Tukey's post-hoc test (a) $p < 0.05$ compared to TCP; (b) $p < 0.05$ compared to OS(-). (For interpretation of the references to colour in this figure legend, the reader is referred to the web version of this article.)

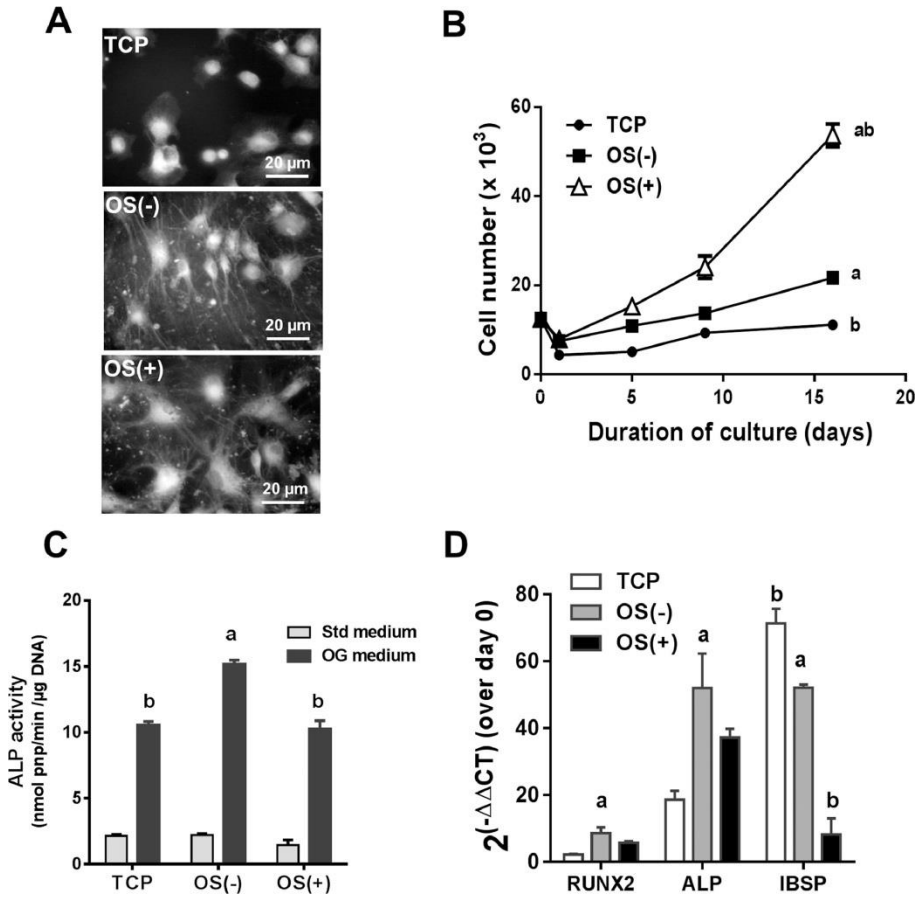

Figure 3. Localization of fluorescently-labelled-BMP-2 bound within either OS(-)or OS(+) 2D-dECMs.

(A) (a) SHG imaging of the fibrillar collagen-rich structure of the OS(-) dECM; (b) Fluorescent observation of BMP-2^{DL488} loaded onto OS(-) dECM; (c) Merged images showing a homogeneous distribution of BMP-2 within the matrix in the form of both soluble protein (appearing as diffuse fluorescence) and protein aggregates (appearing as bright spots). (B) (a,c,e) Observations of the mineralized OS(+)dECM (containing the grainy mineral deposits) using brightfield mode and (b,d,f) of the loaded fluorescent BMP-2^{DL488} revealing a green fluorescent pattern mainly colocalized with the mineral deposits. Light micrographs of BMP-2-containing OS(+) dECMs following treatment with EDTA for 0 s, 180 s and 300 s confirmed the dissolution of the mineralized crystals (a,c,e), while the fluorescence BMP-2^{DL488} imaging showed a strong, but not total, attenuation of the signal (b-d-f). (C) Fluorescence imaging of EDTA treated-OS(+) dECM before (a) and after (b) BMP-2^{DL488} loading. These images are representative results from two separate experiments. (For interpretation of the references to colour in this figure legend, the reader is referred to the web version of this article.)

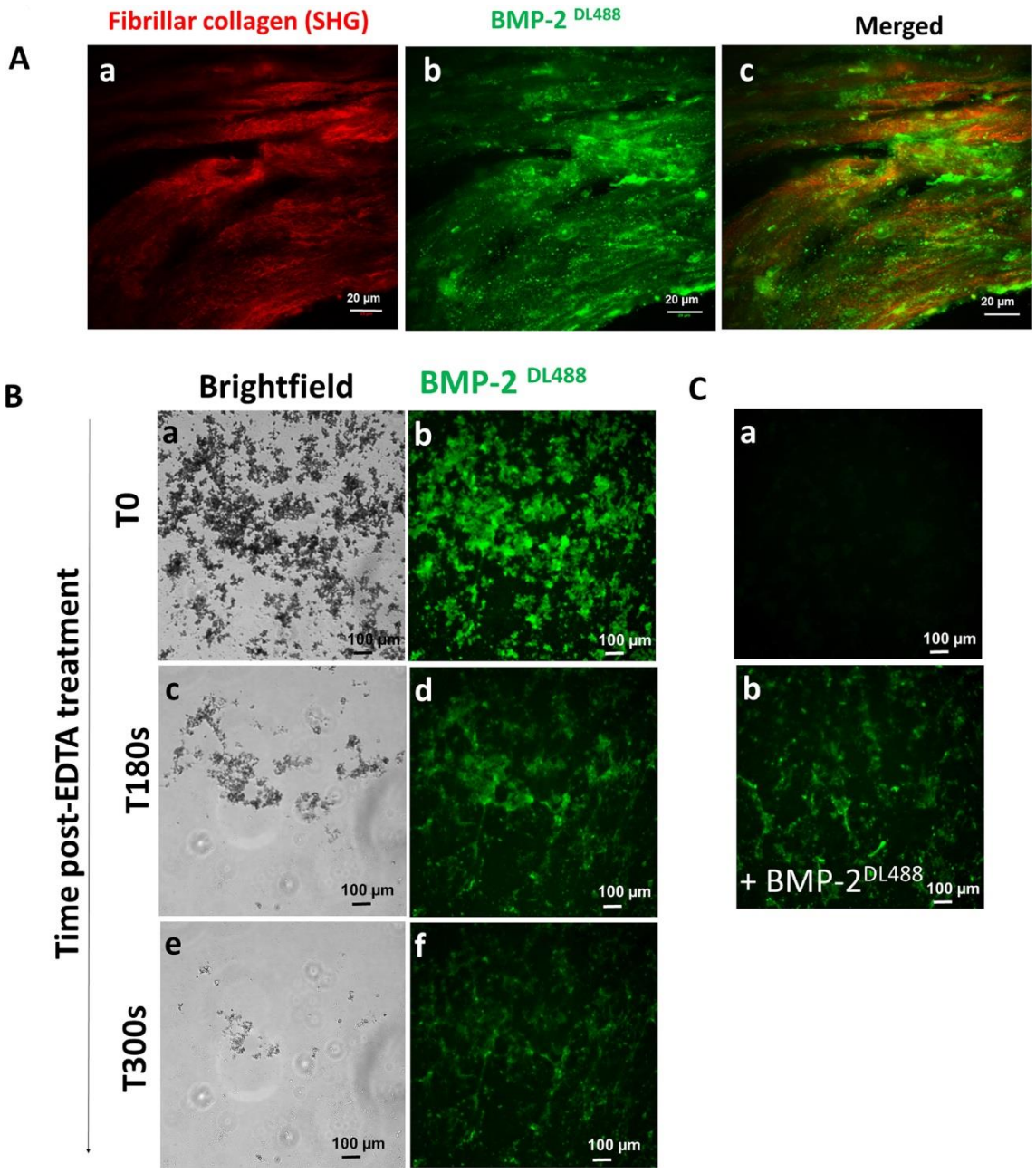

Figure 4. Retention and biological activity of BMP-2 loaded onto 2D-dECMs in vitro.

(A) Quantification of BMP-2 retained within each dECM tested (percentage relative to the initial loaded amount); $n = 5$. (B-C) ALP activity of C2C12 myoblasts cultured on 2D-dECM loaded with BMP-2 either let hydrated (Fresh) or frozen-dried and stored at 4 °C for either 48 h (B) or 11 months (C) $n = 3$. One-way ANOVA with Tukey's post-hoc test. (a) $p < 0.05$ compared to OS(-); (b) $p < 0.05$ compared to Fresh. (For interpretation of the references to colour in this figure legend, the reader is referred to the web version of this article.)

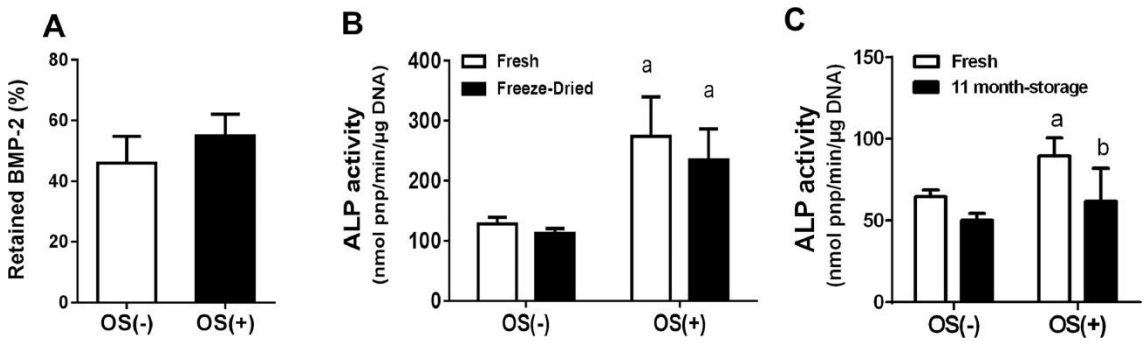

Figure 5. Biochemical characterization of dECMs 3D PCL scaffolds.

(A) Fluorescent microscopy image of Luc-ZsGreen labelled-hMSC 7 days after cell seeding onto a 3D-PCL scaffold (B) Proliferation rate of Luc-ZsGreen labelled-hMSCs cultured onto a 3D-PCL scaffold under standard cell culture conditions; $N = 3$. (C) Representative images of OS(-) and OS(+) dECM 3D-PCL scaffolds stained with Sirius Red/Fast Green FCF and safranin O. (D) Protein, fibrillar collagen and GAG contents in both OS(-) and OS(+) 3D-PCL-dECM; $N = 3$. Unpaired T-Test; (a) $p < 0.05$ compared to OS(-). (E) SEM images of 3D-PCL scaffolds coated with either OS(-) and OS(+) dECMs. (F) Representative images of OS(+) dECM 3D-PCL scaffold stained with Alizarin Red. (For interpretation of the references to colour in this figure legend, the reader is referred to the web version of this article.)

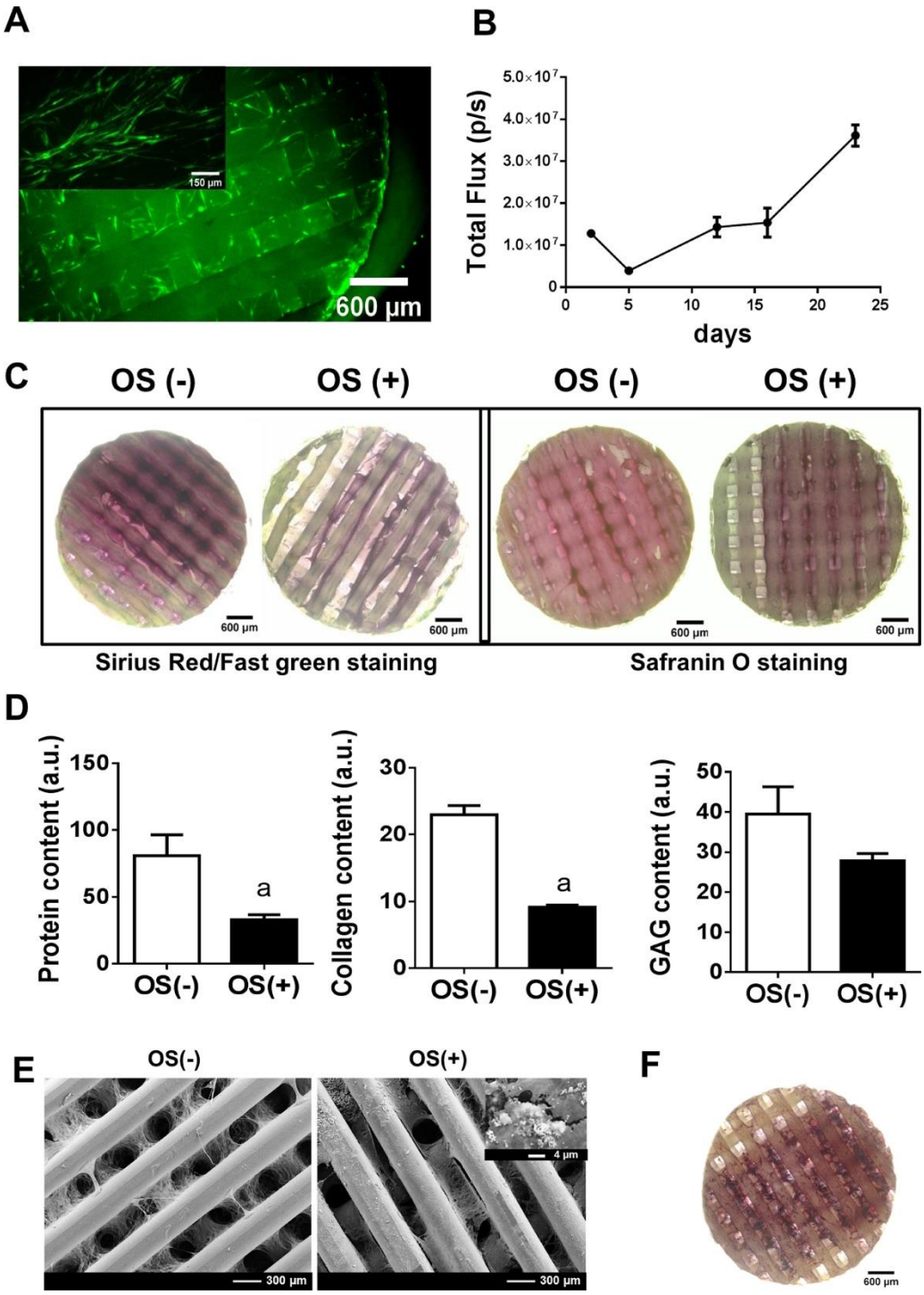

Figure 6. Ectopic bone formation mediated by BMP-2-loaded 3D-PCL-dECM scaffolds.

(A) Representative 3D µCT images of new bone tissue formed in the 3D-PCL scaffolds; the 3D-PCL scaffolds were either only loaded with BMP-2 (Bare), or coated with either OS(-) or OS(+) dECMs and loaded with BMP-2. (B) Time course of bone formation quantified using µCT analysis. $N = 12$ for OS(-) and OS(+) dECMs with BMP-2; $N = 9$ for Bare with BMP-2; $N = 4$ for BMP-2 unloaded-PCL scaffolds. Two-ways ANOVA with Tukey's post-hoc test. (a) $p < 0.05$ compared to Bare; (b) $p < 0.05$ compared to OS(-). (C) Representative, undecalcified, histological cross sections of BMP-2 loaded-3D-PCL scaffolds 4 weeks post-implantation. (D) Histology results illustrating new bone formed in 3D-PCL scaffolds coated with BMP-2-containing dECMs. (b) bone tissue; (o) osteoid; (bm) bone marrow; (PCL) polycaprolactone fibers; arrows point osteoblasts laying down the new formed bone. (For interpretation of the references to colour in this figure legend, the reader is referred to the web version of this article.)

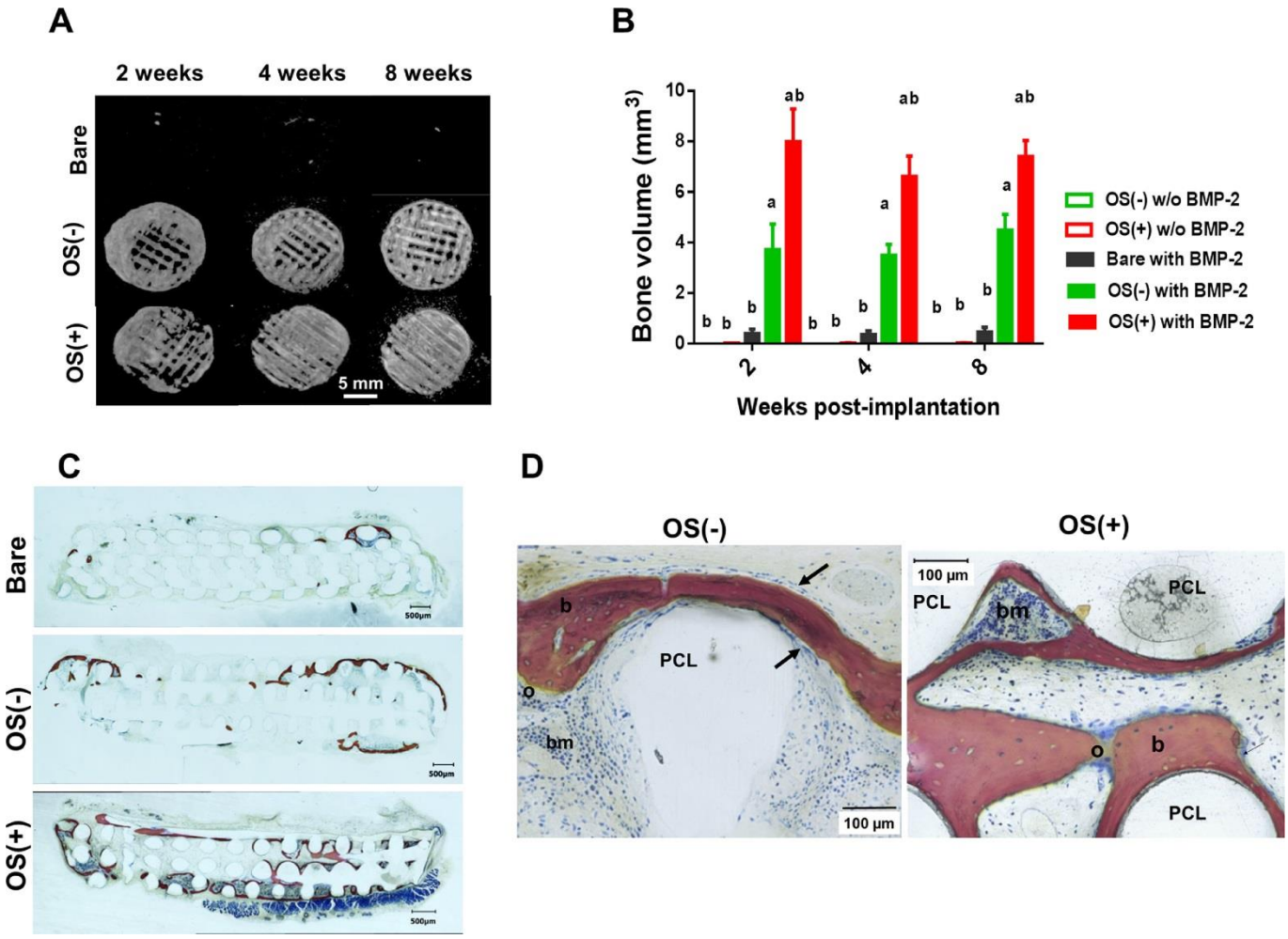

Figure 7. In vivo kinetics of the BMP-2^{DL800} remaining within the 3D-PCL scaffolds.

(A) Fluorescence emitted from BMP-2^{DL800} loaded-3D-PCL scaffolds before their implantation in mice. $N = 6$. (B) Time course of fluorescence imaging of a single representative 3D-PCL scaffold from each group subcutaneously implanted in nude mice. The same pseudocolor scale was used in all images for each implant tested. (C) Time course of the emitted fluorescence (normalized to that obtained at day 0 for each implant tested) post-implantation. $n = 6$. Two-ways ANOVA with Tukey's post-hoc test. $p < 0.05$ compared to Bare; (b) $p < 0.05$ compared to OS(-). (D) Calculated release kinetics parameters: AUC = area under the curve, MRT= mean residence time in days, $t_{1/2}$ = half-life in days. (For interpretation of the references to colour in this figure legend, the reader is referred to the web version of this article.)

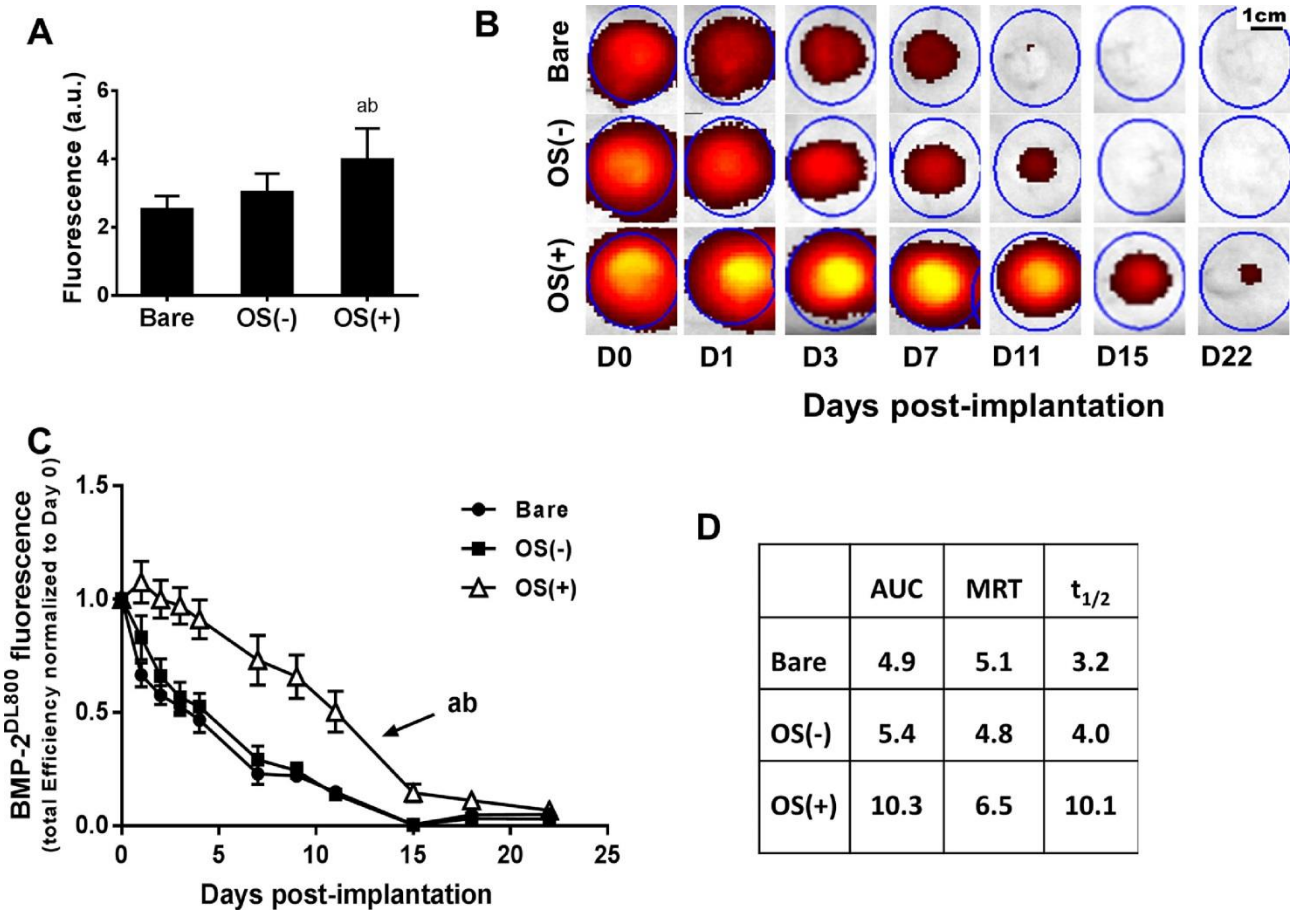

D

	AUC	MRT	$t_{1/2}$
Bare	4.9	5.1	3.2
OS(-)	5.4	4.8	4.0
OS(+)	10.3	6.5	10.1

Figure 8. In vitro and in vivo bioactivities of previously decalcified BMP-2-containing OS(+) dECMs.

(A) ALP activity of C2C12 myoblasts cultured on BMP-2 containing OS(+) 2D-dECM that had been previously either pretreated or not with EDTA. $N = 3$. (B) µ-CT analysis results of new bone formed on BMP-2-containing OS(+) 3D-PCL-dECM either pretreated or not with EDTA, $N = 6$. (For interpretation of the references to colour in this figure legend, the reader is referred to the web version of this article.)

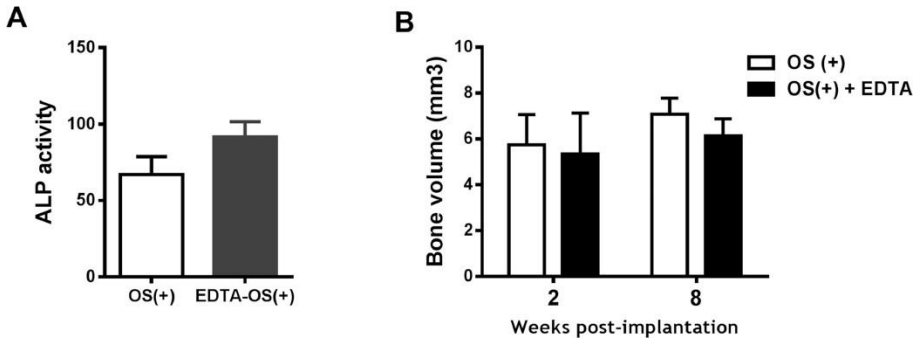

Supplementary Figure 1. Fluorescence intensity profiles of OS(+) 2D-dECM-contained BMP-2^{DL488}.

(A) Fluorescence images 0 s, 30 s, 180 s and 300 s after decalcification treatment with EDTA. Representative images of n = 2. (B) Profiles of fluorescence intensity of BMP-2^{DL488} along the line [A-B], before (0 s) and 30 s, 180 s and 300 s after treatment with EDTA. (C) Profile of the percentage loss of fluorescence measured T300 s after treatment with EDTA (in comparison to results obtained at T0s). The intensity lines within the grey boxes correspond to the mineral-containing areas.